Bioorganic Chemistry 87 (2019) 276–290

Contents lists available at ScienceDirect

Bioorganic Chemistry

journal homepage: www.elsevier.com/locate/bioorg

Interaction of C20-substituted derivative of pregnenolone acetate with copper (II) leads to ROS generation, DNA cleavage and apoptosis in cervical cancer cells: Therapeutic potential of copper chelation for cancer treatment

Atif Zafar[a], Swarnendra Singh[b], Sabahuddin Ahmad[c], Saman Khan[a], Mohammad Imran Siddiqi[c], Imrana Naseem[a,*]

[a] Department of Biochemistry, Faculty of Life Sciences, Aligarh Muslim University, Aligarh 202002, Uttar Pradesh, India
[b] Department of Dermatology and Venereology, All India Institute of Medical Sciences, Ansari Nagar, New Delhi 110 029, India
[c] Molecular and Structural Biology Division, CSIR-Central Drug Research Institute, Lucknow 226031, Uttar Pradesh, India

ARTICLE INFO

Keywords:
Pregnenolone acetate
Tetrazole
Copper
Redox cycling
Apoptosis
DNA damage

ABSTRACT

Cervical cancer is a leading cause of cancer-related deaths among women in developing countries. Therefore, development of new chemotherapeutic agents is required. Unlike normal cells, cancer cells contain elevated copper levels which play an integral role in angiogenesis. Thus, targeting copper via copper-specific chelators in cancer cells can serve as effective anticancer strategy. In this work, a copper chelator pregnenolone acetate nucleus-based tetrazole derivative (ligand-L) was synthesized and characterized by elemental analysis, ESI-MS, ^{1}H NMR and ^{13}C NMR. DNA binding ability of ligand-L was studied using UV–Vis and fluorescence spectroscopy. Fluorescence spectroscopy studies reveal that quenching constant of ligand-L-DNA and ligand-L-Cu(II) were found to be $7.4 \times 10^{3}\ M^{-1}$ and $8.8 \times 10^{3}\ M^{-1}$, respectively. In vitro toxicity of ligand-L was studied on human cervical cancer C33A cancer cells. Results showed that ligand-L exhibit significant cytotoxic activity against cervical cancer C33A cells with IC_{50} value $5.0 \pm 1.8\ \mu M$. Further, it was found that ligand-L cytotoxicity is due to redox cycling of copper to generate ROS which leads to DNA damage and apoptosis. In conclusion, this is the report where we synthesized pregnenolone acetate-based tetrazole derivative against C33A cells that targets cellular copper to induce pro-oxidant death in cancer cells. These findings will provide significant insights into the development of new chemical molecules with better copper chelating and pro-oxidant properties against cancer cells.

1. Introduction

Cervical cancer is the third most common cancer that affects women worldwide with an estimated 530,000 new cases and 275,000 deaths each year in developing countries, out of which India represents one-quarter of the cervix cancer burden globally [1]. The pathological progression of cervical tumorigenesis is associated with high-risk Human Papilloma Virus (HPV) types [2]. Traditional therapeutic approaches for cervical cancer include surgery, radiotherapy and chemotherapy [3]. However, platinum–based chemotherapy against cervical cancer exhibits drug resistance and serious side effects [4,5]. Thus, there is a need to identify and synthesize new chemotherapeutic agents against cervical cancer.

In continuation of our pursuit to design and synthesize new anti-tumor agents against cervical cancer, it is important to note that cancer cells exhibit altered metabolism with elevated copper levels as compared to normal cells [6–8]. Copper is an important redox active metal ion associated with DNA bases, particularly with guanine [9]. Elevated copper in cancer plays an integral role in angiogenesis by functioning as a co-factor of several pro-angiogenic molecules such as VEGF, angiogenin and basic fibroblast growth factor (bFGF) [10,11]. Therefore, development of copper-specific chelators provides a selective approach to target tumor cells. The cytotoxicty of copper complexes towards cancer cells thus arises from their high redox activity to produce reactive oxygen species (ROS) [12]. ROS generation by ligand-copper complexes further leads to metal-driven oxidative DNA damage and cell death [13].

Steroids are a class of naturally occurring organic compounds which exhibit diverse biological activities [14–17]. Steroid-based therapeutics has attracted considerable interest due to various advantages such as

* Corresponding author.
E-mail address: imrananaseem2009@gmail.com (I. Naseem).

https://doi.org/10.1016/j.bioorg.2019.03.031
Received 6 December 2018; Received in revised form 26 February 2019; Accepted 14 March 2019
Available online 19 March 2019
0045-2068/

non-toxic, less vulnerable to drug resistance and high bioavailability in biological systems [18]. Among steroids, pregnenolone derivatives have been synthesized and evaluated for cytotoxicty against several cancer cell lines [19–21]. Addition of heteroatoms (N or O) in the D-ring of pregnenolone skeleton greatly enhances the biological activities of synthesized molecules. Various heterocyclic moieties have been introduced into the core structure of pregnenolone such as pyrazolines, pyrazoles, triazolyl, hydrazones, oximes, thiazoles and hydrazide-hydrazone [19–22]. However, no effort has been made towards the efficient synthesis of pregnenolone-based tetrazole derivatives. Tetrazoles possess wide spread pharmacological properties such as hypotensive, antiviral, antifugal, antimicrobial, antiallergic and anticancer [23–28]. Also, it is important to note that many of the highly effective FDA-approved drugs such as losartan, valsartan, flomoxef and cefonicid contain tetrazole ring system in their active pharmaceutical ingredient [29–33]. Moreover, tetrazole group has also been investigated for its co-ordination properties in metal complexes [34].

Keeping in view the above facts regarding the development of copper-specific chelators for cancer cells, advantages of steroid-based therapeutics and importance of co-ordination properties of tetrazole ring system, we synthesized a pregnenolone acetate-based tetrazole derivative against human cervical cancer C33A cells. Here, we showed that pregnenolone acetate-based tetrazole derivative (ligand-L) showed significant in vitro cytotoxic activity against cervical cancer C33A cells. Ligand-L inhibited cell proliferation and induce apoptosis in C33A cells, and such cell death was prevented to a significant extent by cuprous chelator neocuproine and ROS scavenger *N*-acetyl cysteine (NAC). Ligand-L also induced DNA fragmentation, cell cycle arrest at the G1/S phase, mitochondrial membrane depolarization, up-regulation of p53 and p21 and caspases 9/3 activation. All these effects induced by ligand-L were attenuated by neocuproine and NAC. This indicates that ligand-L cytotoxicity is due to redox cycling of copper to generate ROS which leads to pro-oxidant cell death. These findings will facilitate the future development of new chemical molecules with better copper chelating and pro-oxidant properties against cancer cells.

2. Experimental

2.1. General

Chemicals and solvents used in this study were purchased from Merck, India and Sigma-Aldrich, St. Louis, MO. Melting point was recorded on Buchi melting point apparatus B-545. All the microwave-assisted reactions were performed using an Anton Paar Monowave 300 microwave reactor. IR spectra (KBr discs) were recorded using Perkin Elmer Spectrum Two IR spectrometer and values are given in cm^{-1}. ^{1}H and ^{13}C NMR spectra were run in DMSO-d_6 on a Bruker Avance II 400 NMR spectrometer at 400 MHz and 100 MHz, respectively. Chemical shifts are reported in parts per million (ppm, δ) relative to internal standard tetramethylsilane (TMS). Mass spectra were recorded on a JEOL SX 102/DA-6000 mass spectrometer. Carbon, hydrogen and nitrogen contents were recorded on Perkin Elmer 2400 Series II system. Thin layer chromatography (TLC) plates were coated with silica gel G and exposed to iodine vapours to check the homogeneity as well as the progress of reaction. Sodium sulfate (anhydrous) was used as a drying agent. For the nomenclature of steroid derivative, we used definitive rules for the nomenclature of steroids published by the Joint Commission on Biochemical Nomenclature (JCBN) of IUPAC [35,36]. Calf thymus DNA (ct-DNA) was dissolved in 10 mM Tris-HCl buffer (pH 7.2) at 4 °C with occasional stirring to form homogenous solution. The purity of DNA was determined by recording the absorbance ratio A_{260nm}/A_{280nm}. Since the absorbance ratio of DNA was between 1.8 and 1.9, therefore no further purification was required. The average extinction coefficient value of 6600 M^{-1} cm^{-1} of a single nucleotide at 260 nm was required to determine the concentrations of DNA solutions [37].

2.2. Synthesis of 1-(3β-Acetoxy-pregn-5-ene-20-ylidene)-1H-tetrazol-5yl-acetylhydrazone (Ligand-L)

To a solution of pregnenolone acetate (1 mmol) in ethanol (20 ml), cyanoacetylhydrazine (1 mmol) was added. The reaction mixture was heated under reflux for 2–3 h and allowed to cool at room temperature. The solid product formed upon keeping the reaction mixture overnight was collected by filtration. The precipitate was filtered, dried and monitored through TLC for the purity. TLC revealed just a single spot which proved the presence of a single product i.e. 1-(3β-Acetoxy-pregn-5ene-20-ylidene)-2-cyanoacetylhydrazone (compound 1).

In a sealed tube, sodium azide (1 mmol) and 1.5 equimolar amount of ammonium chloride were added to the stirred solution of compound 1 (1 mmol) in dimethylformamide (DMF) (15 ml). The reaction mixture was subjected to microwave heating on 115 °C for 35–40 min at 300 W. The progress as well as completion of the reaction was monitored by TLC. After completion of the reaction, the excess solvent was removed under reduced pressure by rotary evaporator (Rotavapor, Buchi, USA). The reaction mixture was then taken in diethyl ether, washed with water and dried over anhydrous sodium sulfate. Evaporation of solvents and re-crystallization from methanol afforded the synthesis of ligand- L.

2.2.1. 1-(3β-Acetoxy-pregn-5-ene-20-ylidene)-1H-tetrazol-5yl-acetylhydrazone

Yield: 86%; brown solid; mp 166–168 °C; IR (KBr) cm^{-1}: 3333 (NH), 1732 ($OCOCH_3$), 1688 (C═O), 1654 (C═N), 1610 (C═C), 1368 (C—N). ^{1}H NMR (400 MHz, DMSO-d_6, ppm): 1.31–1.37 (s, 3H), 1.40 (s, 2H), 1.45–1.57 (s, 3H), 1.60–1.81 (m, 5H), 1.84–1.94 (4H), 1.97–2.08 (4H), 2.26 (s, 2H), 4.45–4.47 (m, 2H), 5.35 (t, 1H), 5.76 (s, 2H), 8.21 (s, 1H), δ 9.8 (s, 1H). ^{13}C NMR (100 MHz, DMSO-d_6, ppm): δ = 12.45, 17.04, 23.38, 24.27, 24.46, 25.11, 27.80, 29.57, 31.70, 31.97, 36.70, 36.98, 38.13, 38.34, 38.56, 43.72, 49.77, 56.25, 56.47, 58.69, 63.04, 74.62, 139.94, 154.71, 165.62, 171.87. ESI MS: *m/z* 482.6 [M^+]. Anal.Calcd. for $C_{26}H_{38}N_6O_3$: C, 64.70; H, 7.94; N, 17.41. Found: C, 64.68; H, 7.9; N, 17.45.

2.3. UV–Vis spectroscopy of ligand-L with ct-DNA

UV–Vis spectra of ligand-L in presence and absence of ct-DNA were recorded in the wavelength range 230–600 nm with a UV–Vis spectrophotometer. To 3 ml of reaction volume, fixed concentration of ligand-L (5 μM) was used and titrated against increasing concentration of ct-DNA (0–25 μM).

2.4. UV–Vis spectroscopy of ligand-L with Cu(II)

Absorption spectra of ligand-L in absence and presence of Cu(II) were recorded in the wavelength range 230–600 nm using UV–Vis spectrophotometer (UV-1800, Shimadzu Corp., Tokyo, Japan). To the reaction mixture, fixed concentration of ligand-L (5 μM) was used and titrated against increased concentrations of Cu(II) (0–25 μM) in 10 mM Tris-HCl (pH 7.2).

2.5. Fluorescence studies of ligand-L with Cu(II) and ct-DNA

Fluorescence emission spectra were recorded on a RF-5301PC spectrofluorometer (Shimadzu Corp., Tokyo, Japan). All the reaction mixtures were prepared in 10 mM Tris-HCl (pH 7.2) to determine emission spectra. Ligand-L was excited at 265 nm and emission spectra were recorded in the wavelength range 300–400 nm.

2.6. Detection of ligand-L mediated Cu(II) to Cu(I) conversion

Detection of ligand-L mediated redox cycling of Cu(II) to Cu(I) was analyzed using bathocuproine, which is Cu(I) specific sequestering agent. Bathocuproine binds specifically to Cu(I) form of copper and

when complexed with Cu(I) gives an absorbance maximum at 480 nm [38]. To check the conversion of Cu(II) to Cu(I), reaction mixture was prepared which contained 10 mM Tris-HCl (pH 7.2), 100 μM Cu(II), 300 μM bathocuproine and 50 μM ligand-L and the absorbance was recorded immediately at 480 nm.

2.7. Prediction of drug-likeness (Lipinski's rule of five)

To determine the drug-likeness of ligand-L, physiochemical properties such as octanol-water partition coefficient (log *P*), molecular weight (MW), rotatable bonds, polar surface area, hydrogen bond donors and acceptors were calculated using molinspiration server (www.molinspiration.com/cgi-bin/properties) [39] and ChemAxon (www.chemicalize.org) [40].

2.8. Toxicity studies of Ligand-L

Freshly heparinised blood samples were obtained by venipuncture from a healthy non-smoking volunteer (Atif Zafar: Author himself). The blood was diluted suitably in Ca^{++} and Mg^{++} free PBS. Lymphocytes were isolated from blood using Histopaque 1077 (sigma) and the cells were finally suspended in RPMI 1640. Isolated lymphocytes were checked for their viability before the start of the reaction using Trypan blue exclusion test [41].

Toxicity of ligand-L was analysed by using 3-(4,5-dimethylthiazol-2-yl)-2,5-diphenyl tetrazolium bromide (MTT) assay [42]. Freshly isolated lymphocytes were plated in 96-well flat bottom tissue culture plate at a concentration of 1×10^4 cells/well. Lymphocyte samples were incubated with increasing concentration of ligand-L (25–100 μM) at 37 °C in 5% CO_2 for 24 h. After 24 h treatment, 10 μl of MTT solution (5 mg/ml stock solution) was added in each well, re-incubated for 3 h at 37 °C until formazan blue crystal developed. Afterwards, 100 μl of DMSO was added to each well to solubilise the crystals. Plates were then read using ELISA plate reader at the wavelength 570 nm (Bio Tek Instruments Inc., USA). Also, apoptosis induction in lymphocytes by increasing concentration of ligand-L (25–100 μM; incubation time 24 h) was analysed by flow cytometry using Annexin V-FITC Detection Kit (Sigma-Aldrich, St. Louis, USA).

2.9. Cell culture and antibodies

Human cervical cancer cell line C33A was purchased from American Type Culture Collection (ATCC, Manassas, VA). C33A cells were cultured in Dulbecco's Modified Eagle Medium (DMEM, Sigma-Aldrich, St. Louis, MO) supplemented with 10% heat-inactivated fetal bovine serum (FBS, Sigma-Aldrich, St. Louis, MO) and 1% penicillin and streptomycin. Cells were grown in tissue culture flasks at 37 °C in an atmosphere of 5% CO_2 incubator and were checked for mycoplasma contamination by mycoplasma PCR detection kit (Sigma-Aldrich, St. Louis, MO). Antibodies to Bcl-2, Bax, caspase-3, caspase-9, cyclin E, CDK2, p53, p21 and β-actin were obtained from Santa Cruz Biotechnology Inc. (Santa Cruz, CA, USA).

2.10. Cellular viability assay and IC_{50} determination

Cell viability was assayed using MTT assay [42]. For this experiment, 1×10^4 C33A cells were seeded into 96-well plate overnight for adherence. Cells were then treated with increasing concentrations of ligand-L for 24 h at 37 °C in 5% CO_2. After 24 h treatment, 20 μl of MTT solution (5 mg/ml stock solution) was added in each well, re-incubated for 3 h at 37 °C until formazan blue crystal developed. Thereafter, the medium was completely aspirated and 100 μl of DMSO was added to solubilise the formazan crystals. Plates were then read using ELISA plate reader at the wavelength 570 nm (Bio Tek Instruments Inc., USA). IC_{50} value for ligand-L was calculated by determining the concentration that causes 50% inhibition of cell growth of C33A cells. Later, at IC_{50} concentration of ligand-L, MTT assay was performed in the presence of membrane permeant copper chelator neocuproine (50 μM) and ROS scavenger *N*-acetyl cysteine (NAC) (1 mM).

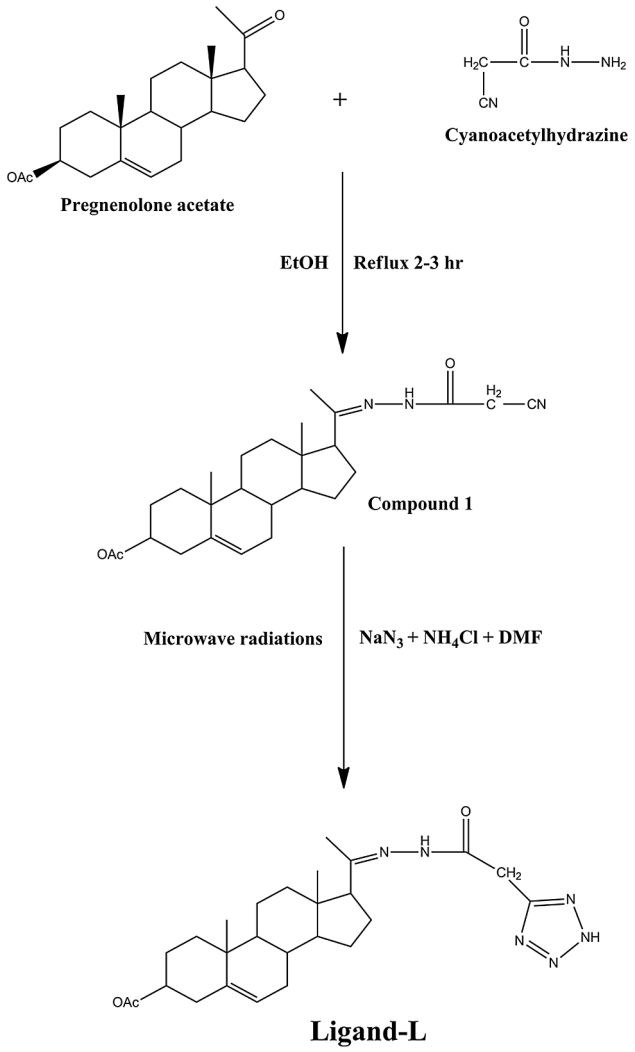

Fig. 1. Scheme 1: Synthetic route for the synthesis of Ligand-L.

2.11. Evaluation of ROS generation

Intracellular ROS generation namely hydrogen peroxide (H_2O_2) and superoxide anion ($O_2^{\cdot-}$) were assessed in treated C33A cells using DCFH-DA and DHE probes, respectively [43,44]. Briefly, C33A cells (1×10^4 /well) were seeded in 96-well black bottom culture plates and allowed to adhere overnight and then treated with IC_{50} concentration of ligand-L and also with neocuproine or NAC in different sets of experiments at 37 °C in 5% CO_2 for 24 h. After complete incubation, the cells were stained with DHE (20 μM) for 20 min and DCFH-DA (30 μM) for 30 min at 37 °C. The reaction was aspirated and replaced by 200 μl of phosphate buffer saline (PBS). Plates were then placed on the shaker for 15 min at room temperate in the dark. For quantitative ROS analysis, fluorescence intensity was measured by multi-detection micro-plate reader (Bio Tek Instruments Inc., Winooski, VT, USA) at 485 nm (excitation wavelength) and 528 nm (emission wavelength) for DCFH-DA and 596 nm (excitation wavelength) and 620 nm (emission wavelength) for DHE. The values were expressed as the percentage fluorescence intensity relative to control cells.

Hydroxyl radical generation by ligand-L alone (at IC_{50} concentration) and in presence of Cu(II) ions (10 μM) was detected by the method

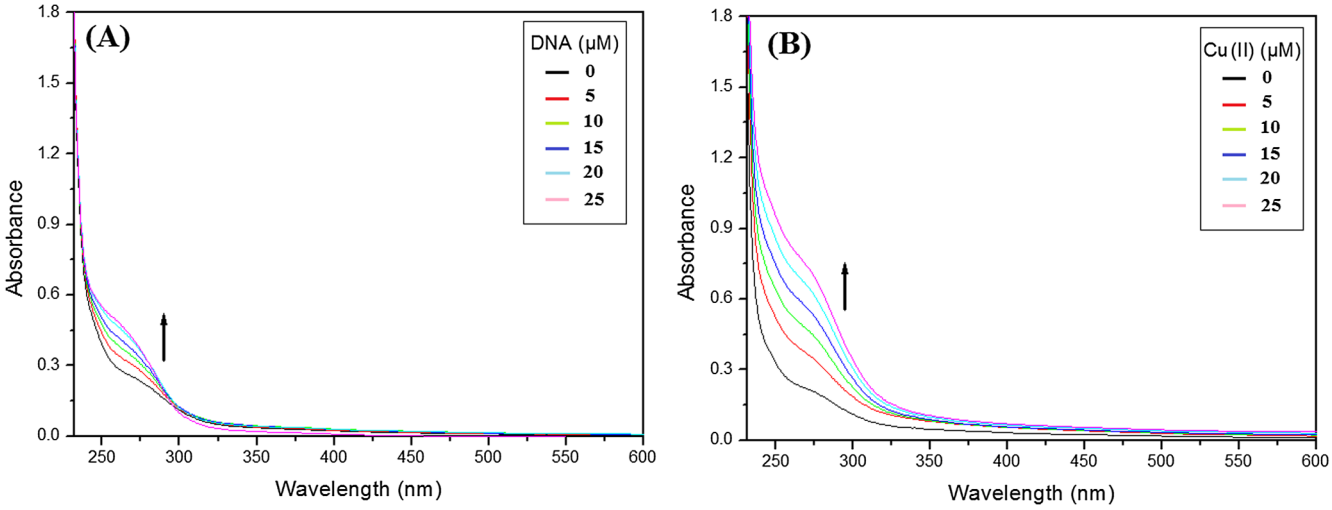

Fig. 2. Effect of increasing concentrations of (A) ct-DNA (5–25 μM) and (B) Cu(II) (5–25 μM) on the absorption spectra of ligand-L (5 μM). Black coloured arrow indicates the hyperchromic (upward arrow) shifts on Ligand-L-DNA and Cu(II)-Ligand-L interactions.

of Quinlan and Gutteridge [45]. Calf thymus (CT) DNA (300 μg) was used as a substrate and the generation of malondialdehyde from deoxyribose radicals was assayed by recording the absorbance at 532 nm.

2.12. Apoptosis analysis via Annexin V-FITC/PI assay

Apoptosis detection by flow cytometry was carried out using the Annexin V-FITC Detection Kit (Sigma-Aldrich, St. Louis, USA). Cells were seeded in 6-well plate at a concentration of 1×10^6 cells per well. Next, the cells were treated with IC_{50} concentration of ligand-L and ligand-L + Neocuproine (50 μM) or NAC (1 mM) in different sets of experiments for 24 h. After incubation, the cells were collected and immediately suspended in the 1X binding buffer and subsequently stained with 5 μl Annexin V-FITC conjugate and 10 μl propidium iodide (PI) solution. Cell mixture was incubated for 15 min at room temperature. Data acquisition was performed on a FACSVerse flow cytometer (BD Biosciences, San Jose, CA). The acquired data was analyzed using FlowJo Software (Treestar, Ashland, OR). Early and late apoptotic cells were expressed as percentage of total number of cells. For each sample, 10,000 cells were analyzed.

2.13. Cell cycle arrest analysis

Cell cycle arrest analysis was carried out by flow cytometry. C33A cells (2×10^5 /well) were grown in a 6-well culture plate and exposed to IC_{50} concentration of ligand-L and ligand-L + Neocuproine (50 μM) or NAC (1 mM) in different sets of experiments for 24 h. After 24 h incubation, the cultured cells were harvested and washed with PBS. Later, the cells were fixed in ice-cold 70% ethanol at −20 °C overnight. Following fixation, the cells were washed with PBS and treated with RNase (200 μg/ml) and Triton X-100, and were then stained with propidium iodide (PI) (Sigma, USA) in the dark at room temperature for 30 min. Cell cycle phase distribution was analysed by flow cytometry and the percentage of cells in various phases (G_0, G_1, S and G_2/M phases) was determined by FlowJo Software (Treestar, Ashland, OR).

2.14. Assessment of mitochondrial membrane potential ($\Delta\Psi_m$)

Cationic, lypophilic dye 5,5′,6,6′-tetrachloro-1,1′,3,3′-tetraethylbenzimidazol-carbocyanine iodide (JC-1) has been used to study the loss of the mitochondrial potential during apoptosis [46]. Briefly, 1×10^6 cells were treated with IC_{50} concentration of ligand-L and ligand-L + Neocuproine (50 μM) or NAC (1 mM) in different sets of experiments for 24 h. Following treatment, the cells were harvested and suspended in 1 ml PBS. To each tube, 10 μl of 200 μM of JC-1 dye is added and incubated the cells at 37 °C, 5% CO_2 for 20 min after which they were analyzed with flow cytometry (FACSVerse flow cytometer) with 10,000 events were recorded per analysis.

2.15. Morphological assessment of cell death by phase contrast and fluorescence microscopy

Approximately 1×10^5 cells were seeded in 6-well culture plate and were exposed to IC_{50} concentration of ligand-L and ligand-L + Neocuproine (50 μM) or NAC (1 mM) in different sets of experiments for 24 h. After complete incubation, the cells were examined using a phase contrast inverted microscope to identify the morphological features of apoptotic cells such as cell-volume shrinkage and formation of apoptotic bodies [47].

Apoptosis induction by ligand-L in treated cells was also analyzed by analysing the nuclear morphology using DAPI staining. Treated cells (1×10^5/well) were incubated in DAPI (10 μg/ml) solution for 20 min at room temperature in the dark. After staining, the images were captured using a fluorescent microscope (Nikon ECLIPSE Tis, Japan) for determination of nuclear morphological changes. Typical result from three experiments is shown.

2.16. Colony formation assay

C33A cells were seeded into 6-well plates at a density of 1200 cells per well in triplicate. Cells were exposed to IC_{50} concentration of ligand-L and ligand-L + Neocuproine (50 μM) or NAC (1 mM) in different sets of experiments for 24 h. After 24 h, the medium was replaced with the fresh medium without any compound. After incubation at 37 °C for 14 days, cells were fixed using 2.5% glutaraldeyde, stained with 0.5% toluidine blue solution, and the visible colonies were then photographed using eclipse TS100 light microscope (Nikon Corporation, Tokyo, Japan).

2.17. Western blot analysis

C33A cells were exposed to IC_{50} concentration of ligand-L and ligand-L + Neocuproine (50 μM) or NAC (1 mM) in different sets of experiments for 24 h. After incubation, cell were harvested and lysed with ice-cold lysis buffer (150 mM NaCl, 50 mM of pH 7.4 Tris, 1 mM EDTA,

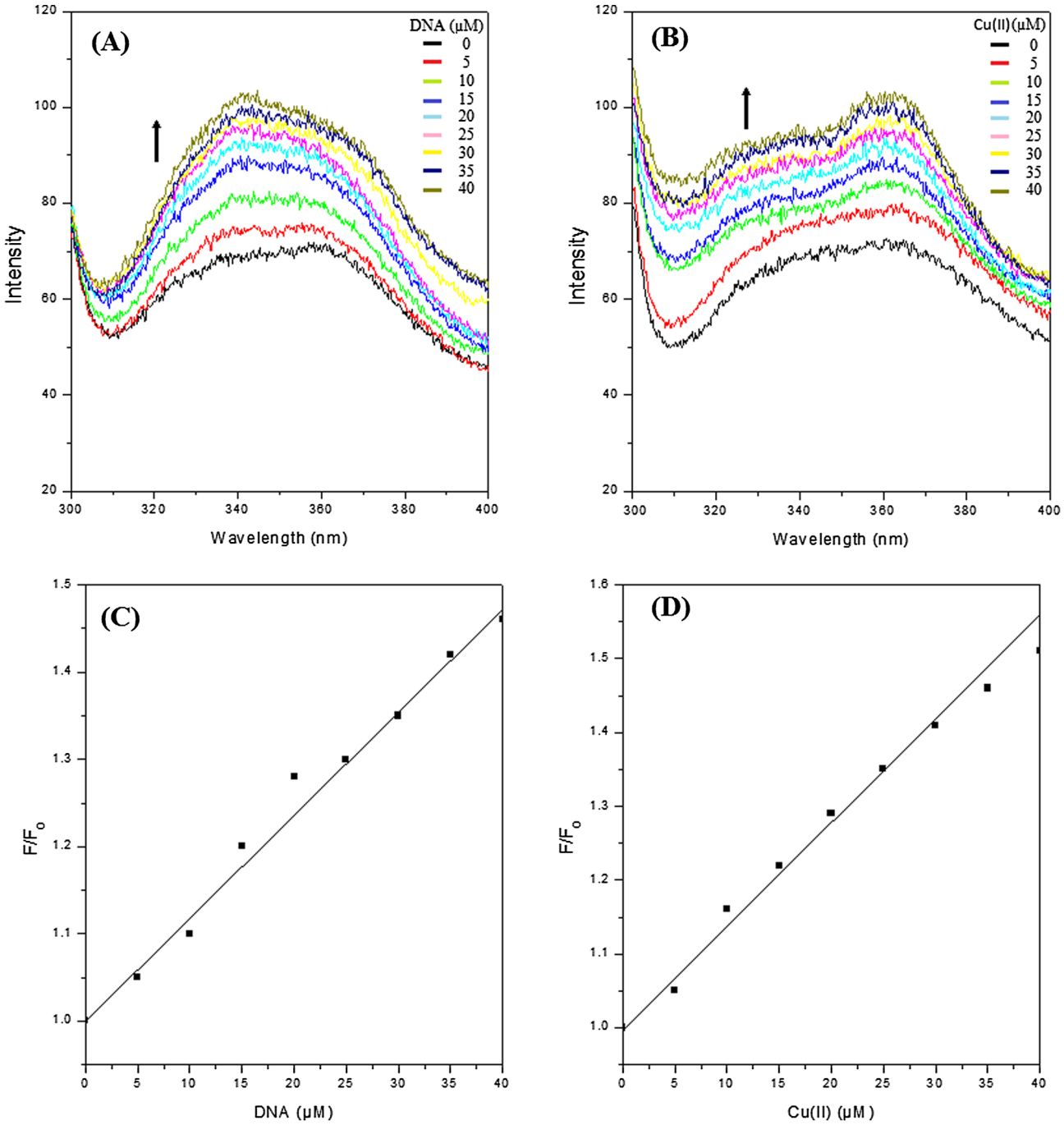

Fig. 3. Effect of increasing concentrations of (A) ct-DNA (5–40 μM) and (B) Cu(II) (5–40 μM) on the fluorescence emission spectra of Ligand-L. Ligand-L (5 μM) was excited at 265 nm in the presence of increasing ct-DNA and Cu(II) concentrations and the emission spectra were recorded between 300 and 400 nm. Stern-Volmer plot for interaction of ligand-L with ct-DNA (C) and Cu(II) (D). Binding constant was obtained from the slope.

1% Triton X-100, 0.5% SDS, 0.01% PMSF). After centrifugation, protein was quantified and 40 μg of protein was resolved on 10–15% SDS-PAGE and transferred to polyvinylidene difluoride (PVDF) membrane. Membranes were blocked with 5% non-fat dry milk in TBST (0.1% Tween-20 in Tris-buffered saline) for 60 min and then incubated with primary antibody for Bcl-2, Bax, caspase-3, caspase-9, cyclin E, CDK2, p53, p21 and β-actin at 4 °C overnight. After primary antibody incubation, membranes were washed three times with TBST and then incubated with HRP-conjugated secondary antibody for 1 h. The membranes were then washed three times in TBST and protein expression was visualised by ECL detection reagent and developed by exposure to X-ray films.

2.18. Molecular docking studies

The three dimensional (3D) chemical structure of pregnenolone acetate derivative (ligand-L) was obtained and minimised using Sybyl-X (v.2.1.1). Molecular docking was performed to predict binding-site and binding-mode of ligand-L with double-stranded B-DNA (PDB: 1BNA). AutoDock (v4.2) [48] suit incorporated in MGL tools (v1.5.6) [49] was used to perform docking. Docking was performed in two consecutive stages. At first stage, the preferred binding site was indentified. The input 'grid parameter' file was modified and adjusted to 70 * 50 * 100 points in XYZ dimensions, respectively, with default spacing of 0.375 Å to cover the complete DNA molecule. Likewise, the input 'docking

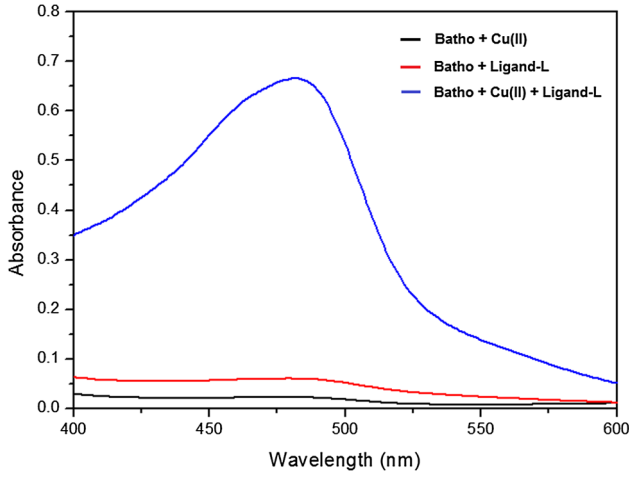

Fig. 4. Reduction of Cu(II) to Cu(I) by ligand-L. Ligand-L induced conversion of Cu(II) to Cu(I) was detected by the formation of bathocuproine-Cu(I) complex. Absorption spectra were recorded between 400 and 600 nm. No characteristic peak was observed in case of bathocuproine + Cu(II) and bathocuproine + ligand-L. Reaction mixture contained the following: 300 μM bathocuproine + 100 μM Cu(II), 300 μM bathocuproine + 50 μM ligand-L and 300 μM bathocuproine + 50 μM ligand-L + 100 μM Cu(II).

parameter' file was slightly modified. The numbers of Genetic Algorithm (GA) runs were set to 100. Using clustering approach, best pose from most populated cluster was saved and considered for second stage. The grid for the second stage was localized to the binding site of the best pose obtained from stage one and then again molecular docking was performed for 100 GA runs. Best pose from the most populated cluster of second stage resembles preferred binding mode of ligand-L with B-DNA. The complex was saved and considered for visualisation and molecular dynamics (MD) simulations. Molecular visualisation was aided by UCSF-Chimera (v1.8.1) [50]. LIGPLOT^{+} (v1.4.5) was also used to identify hydrophobic interactions and hydrogen bonding between ligand-L and B-DNA [51].

2.19. Molecular dynamics (MD) simulations

The stability of the docked complex was evaluated via MD simulations. Simulations were performed over server facilitated with AMD Opteron™ Processor 6386 SE using the GROningen MAchine for Chemical Simulations (GROMACS) v5.0.7 package [52]. The complex was separated into two PDB files, one each for ligand-L and B-DNA. The system topology of separated PDB files was prepared individually in two different steps. DNA topology was prepared considering 'CHARM27 all-atom' force field [53] and using the module 'pdb2gmx' of GROMACS. The ligand topology was prepared over SwissParam server [54]. The solvated system had a net charge of –22.0. Therefore, 22 sodium ions were added to neutralize the system. The neutralized, solvated system was then minimized using the steepest descent method. After energy minimization, position restraint dynamics, also known as equilibration run, was performed in two consecutive steps, NVT (Number of particles, Volume and Temperature) equilibration and NPT (Number of particles, Pressure and Temperature) equilibration. Soon after the system was equilibrated, a 20 ns (ns) long production simulation (MD run) was started with a 2 fs (fs) time step at a pressure of 1 bar, and a temperature of 300 K, to confirm stability of the given system. The interaction energy and intermolecular hydrogen bonds of the system were calculated using the modules 'gmx energy' and 'gmx hbond', respectively. The trajectories of simulations were plotted using Gnuplot (v4.6) (http://sourceforge.net/projects/gnuplot).

2.20. Statistical analysis

Experimental values were expressed as mean ± SEM of three independent experiments. Data was analysed by one way- analysis of variance (ANOVA) using GraphPad Prism 5.01 (California, USA) to examine statistically significant differences. P-values < 0.05 were considered statistically significant.

3. Results

3.1. Chemistry

The synthetic pathway for the preparation of ligand-L has been

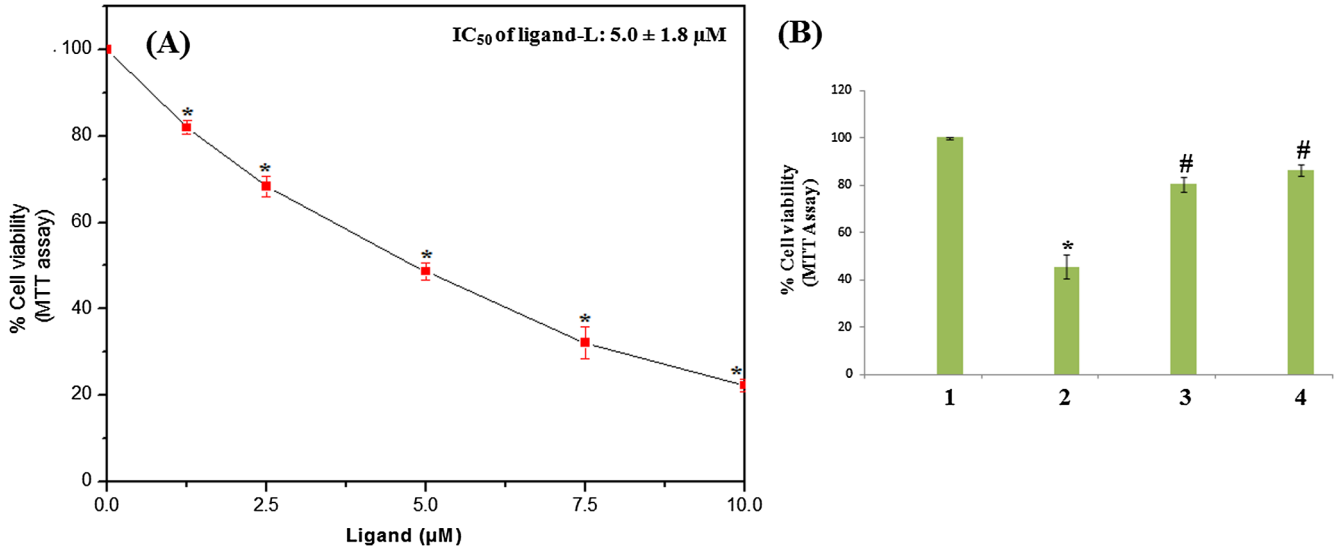

Fig. 5. Percent cell viability of treated C33A cervical cancer cells measured by MTT assay. (A) Effect of increasing concentrations of ligand-L on cell viability of C33A cervical cancer cell line and determination of IC_{50} value of ligand-L for 24 h. Values expressed as mean ± SEM of three independent experiments. *P < 0.05 with respect to control group. (B) Effect of copper chelator neocuproine and ROS scavenger NAC on ligand-L induced cell growth inhibition in C33A cervical cancer cells for 24 h and analysed by MTT assay. (1) Control (2) ligand-L (5 μM) (3) ligand-L (5 μM) + Neocuproine (50 μM) (membrane permeable Cu(II) chelator) (4) ligand-L (5 μM) + NAC (1 mM) treatment. Values expressed as mean ± SEM of three independent experiments. *P < 0.05 with respect to control group and $^{\#}$P < 0.05 with respect to 5 μM ligand-L treated cells.

depicted in "scheme 1" (Fig. 1). The compound was obtained in excellent yield (86%) with high degree of purity. The structure of ligand-L was established on the basis of IR, ^{1}H NMR, ^{13}C NMR, ESI-MS and elemental analysis. The characterisation studies have been in good corroboration with the expected structural framework of ligand-L. IR spectrum of ligand-L displayed characteristic signals at 3333.50 cm^{-1} and 1688.40 cm^{-1} due to the presence of –NH (tetrazole ring) and C═O group, respectively, while the bands at 1654.43 cm^{-1} and 1368 cm^{-1} were ascribed to C═N and C—N, respectively (Supplementary Fig. S1). In ^{1}H NMR spectral analysis, ligand-L exhibited singlet (D_2O exchangeable) at δ 9.8 ppm assigned to —NH of amide group and singlet at δ 8.21 ppm indicates proton of tetrazole ring (Supplementary Fig. S2). A singlet peak resonating at δ 2.26 ppm corresponding to two protons, has been attributed to methylene protons (—CH_2) of —$COCH_2$ group, whereas a singlet at δ 2.51 ppm assigned to —$OCOCH_3$ group (signal for pregnenolone moiety) (Supplementary Fig. S2). In ^{13}C NMR spectral study, the absorption bands resonating at around δ 171.87, δ 165.62 and δ 154.71 correspond to acetoxy (pregnenolone moiety), —CONH and C═N groups, respectively (Supplementary Fig. S3). These data confirmed the presence of hydrazone tetrazole-ring system in ligand-L. The mass spectral analysis was also found to be in good conformity with the proposed structure.

3.2. Formation of complexes involving ct-DNA/Cu(II) with ligand-L

Interaction of ligand-L with ct-DNA and Cu(II) was analyzed by UV–Vis spectroscopy. Fig. 2A shows the effect of addition of increasing concentration of ct-DNA to absorption spectra of ligand-L. On addition of increasing concentrations of ct-DNA, hyperchromism was observed in a dose-dependent manner with no significant shift in the position of absorbance maximum peak of ligand-L. Similarly, absorption spectra of ligand-L exhibited hyperchromism on addition of increasing Cu(II) concentrations (Fig. 2B). These results confirm the binding of ligand-L to ct-DNA and Cu(II) ions.

Steady state fluorescence spectroscopy was also used to detect the interaction of ligand-L to ct-DNA and Cu(II) ions. Fig. 3A and B shows the effect of addition of increasing concentration of ct-DNA and Cu(II) ions on the fluorescence emission spectra of ligand-L excited at 265 nm. On addition of ct-DNA and Cu(II) to ligand-L solution, increase in fluorescence was observed with no significant shift in λ_{max} emission of ligand-L. The increase in fluorescence intensity (hyperchromism), thus, confirmed the binding of ligand-L to ct-DNA and Cu(II) ions. To further understand the interaction of ligand-L with DNA and Cu(II) ions, binding constant (K_{sv}) was obtained from Stern-Volmer equation:

$$F_0/F = 1 + K_{sv}[Q] \quad (1)$$

where F_0 and F are the fluorescence intensities in the absence and

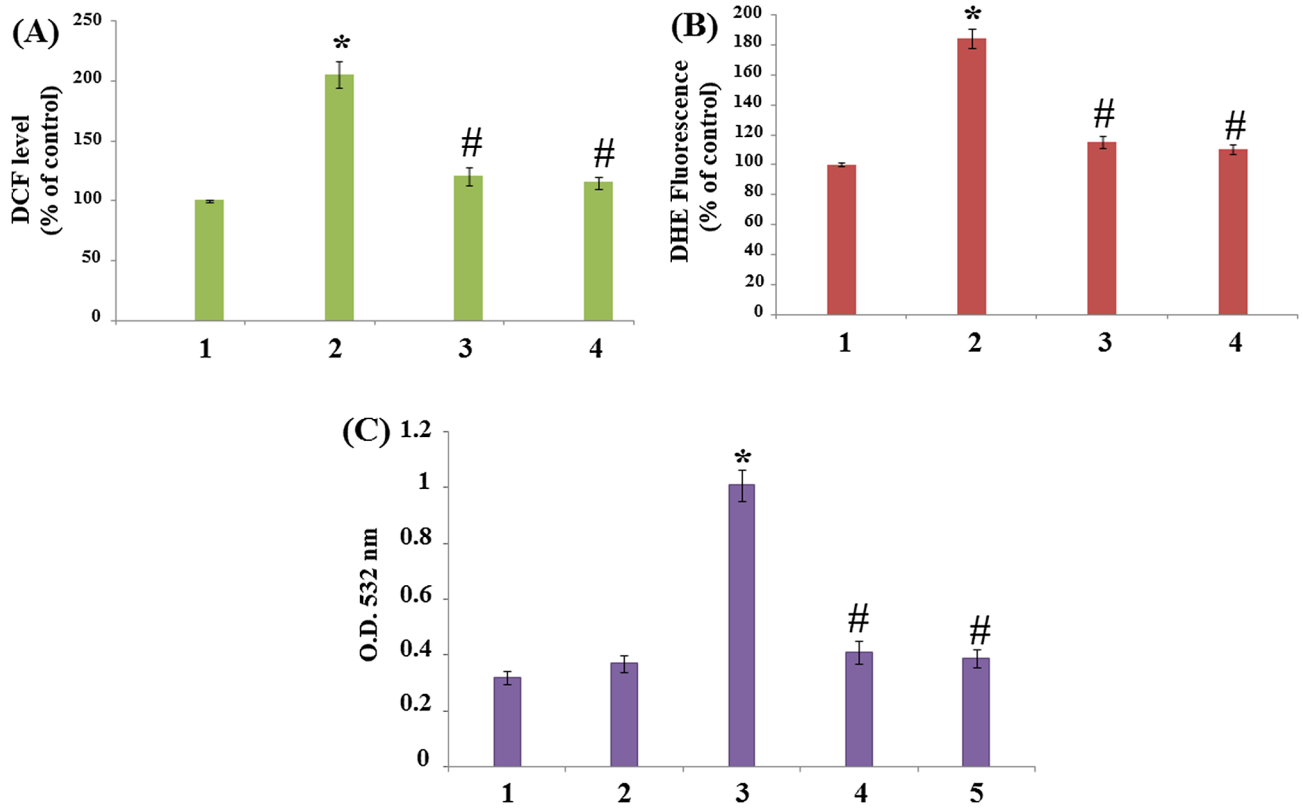

Fig. 6. Detection of ROS generation. (A) Bar graph representation of data from DCFH-DA assay on treated C33A cervical cancer cells. (1) Control (2) ligand-L (5 μM) (3) ligand-L (5 μM) + Neocuproine (50 μM) (membrane permeable Cu(II) chelator) (4) ligand-L (5 μM) + NAC (1 mM) treatment. Values are expressed as percentage of fluorescent intensity relative to the control. Values are expressed as mean ± SEM of three independent experiments. *P < 0.05 with respect to control group and #P < 0.05 with respect to 5 μM ligand-L treated cells. All incubations were carried out for 24 h at 37 °C. (B) Bar graph representation of data from DHE assay on treated C33A cervical cancer cells. (1) Control (2) ligand-L (5 μM) (3) ligand-L (5 μM) + Neocuproine (50 μM) (membrane permeable Cu(II) chelator) (4) ligand-L (5 μM) + NAC (1 mM) treatment. Values are expressed as percentage of fluorescent intensity relative to the control. Values are expressed as mean ± SEM of three independent experiments. *P < 0.05 with respect to control group and #P < 0.05 with respect to 5 μM ligand-L treated cells. All incubations were carried out for 24 h at 37 °C. (C) Bar graph representation of data from hydroxyl radical assay using ct-DNA as substrate. (1) Control (2) ligand-L (5 μM) (3) ligand-L (5 μM) + Cu(II) (10 μM) (4) ligand-L (5 μM) + Cu(II) (10 μM) + Neocuproine (50 μM) (5) ligand-L (5 μM) + Cu(II) (10 μM) + thiourea (0.65 mM). All incubations were carried out for 2 h at 37 °C. Values are expressed as mean ± SEM of three independent experiments. *P < 0.05 with respect to control group and #P < 0.05 with respect to 5 μM ligand-L + 10 μM Cu(II) treated set.

presence of ctDNA or Cu(II) ions, respectively and [Q] is the concentration of ctDNA or Cu(II) ions in the solution. The binding constant (K_{sv}) was determined by plotting the ratio of fluorescence intensity (F/F_0) in the presence and absence of ctDNA or Cu(II) ions as a function of increasing concentrations of DNA or Cu(II) ions. K_{sv} values were calculated from the slope of Fig. 3C and D and found to be $7.4 \times 10^3\ M^{-1}$ and $8.8 \times 10^3\ M^{-1}$ for ctDNA and Cu(II) ions, respectively.

3.3. Ligand-L induces Cu(II) to Cu(I) conversion

Reduction of Cu(II) to Cu(I) by ligand-L was detected using bathocuproine, which binds specifically to the reduced form of copper, Cu (I). Bathocuproine-Cu(I) complex gives a maximum absorbance at 480 nm. As evident from Fig. 4, ligand-L + Cu(II) react to form Cu(I), which forms a complex with bathocuproine and gives absorbance maxima at 480 nm. Whereas bathocuproine-Cu(II) and bathocuproine-ligand-L solutions exhibit no characteristic peaks at 480 nm, suggesting ligand-L can cause redox cycling of copper ions.

3.4. In silico study of ADME/T prediction

For a compound to be orally active (drug-likeness), it should follow Lipinski 'Rule of five' which includes the following parameters: (1) Mass < 500; (2) Octanol-water partition coefficient (logP) ≤ 5; (3) Rotatable bonds ≤ 10; (4) Polar surface area ≤ 150 Å^2; (5) Hydrogen bond acceptors ≤ 10; (6) Hydrogen bond donors ≤ 10. Ligand-L under investigation follows all the parameters under 'Rule of five' (no violations) calculated via molinspiration and chemicalize.org servers, and revealed higher tendency of ligand-L towards drug-likeness (Supplementary Table S1).

3.5. Toxicity analysis of ligand-L on C33A cells and lymphocytes

To measure the cytotoxic potential of ligand-L against cervical C33A cells, MTT assay was performed. Treatment with ligand-L inhibited viability of C33A cells in a dose-dependent manner with IC_{50} value of 5.0 ± 1.8 μM (Fig. 5A). Using the observed IC_{50} value (5.0 μM) of ligand-L, MTT assay was also performed in the presence of neocuproine and NAC (Fig. 5B). Neocuproine, a membrane permeant copper chelator significantly inhibited cellular toxicity of ligand-L (Fig. 5B). On the other hand, NAC (ROS scavenger) suppressed the ligand-L effect on C33A cells (Fig. 5B). These results indicated that ligand-L engages in redox cycling of Cu(II) which in turn generate ROS and induce cell death in C33A cells. In addition, toxicity of ligand-L was also checked on human lymphocytes via MTT and Annexin-V FITC/PI assays. Results revealed that ligand-L at concentrations 25–100 μM did not affect the cell viability of treated lymphocytes (Supplementary Fig. S4). Similarly, increasing concentrations of ligand-L (25–100 μM) resulted in no significant apoptosis (% total annexin positive cells) as compared to control lymphocytes (Supplementary Table S2). These results suggest that ligand-L exhibits no significant toxicity at the tested concentrations on human lymphocytes.

3.6. Ligand-L induces intracellular ROS generation

ROS generation was assessed after ligand-L treatment in cervical cancer C33A cells. To detect ROS generation, treated C33A cells were incubated with DCFH-DA, which is an indicator of cellular hydrogen peroxide production. Quantitative ROS (hydrogen peroxide) measurement via multi-plate reader showed that ligand-L (at IC_{50} concentration) elevates ROS production significantly, i.e. 2.05-fold increase as compared to control (Fig. 6A). Further, ROS (hydrogen peroxide)

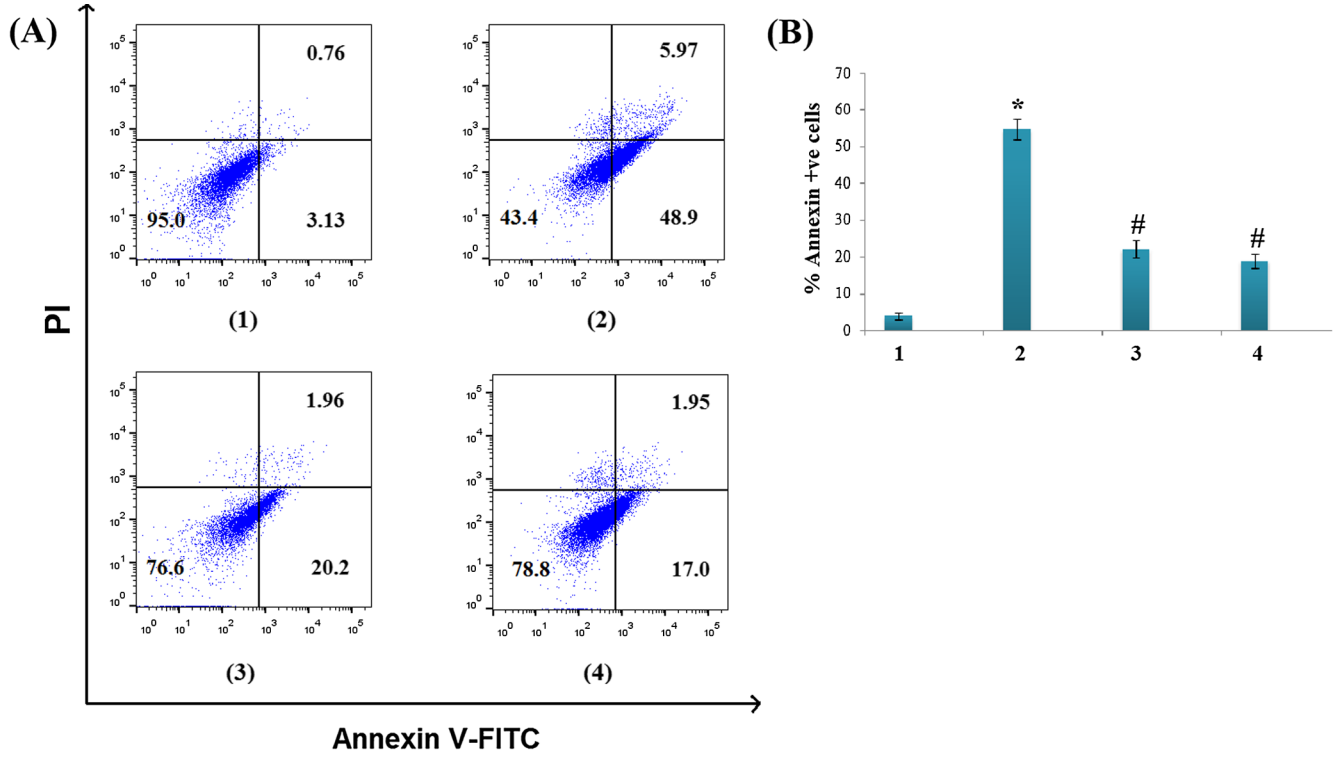

Fig. 7. Ligand-L induces apoptosis in C33A cervical cancer cells analysed via Annexin-V/PI assay. (A) Flow cytometry analysis of treated C33A cervical cancer cells. (1) Control (2) ligand-L (5 μM) (3) ligand-L (5 μM) + Neocuproine (50 μM) (membrane permeable Cu(II) chelator) (4) ligand-L (5 μM) + NAC (1 mM) treatment. Representative figures showing population of viable (annexin V- PI-), early apoptotic (annexin V + PI-) and late apoptosis (annexin V + PI +) cells. (B) Bar graph showing % population of Annexin V + cells after different treatments. Sets (1)-(4) correspond to the treatments mentioned above. Values are expressed as mean ± SEM of three independent experiments. *P < 0.05 with respect to control group and #P < 0.05 with respect to 5 μM ligand-L treated cells. All incubations were carried out for 24 h at 37 °C.

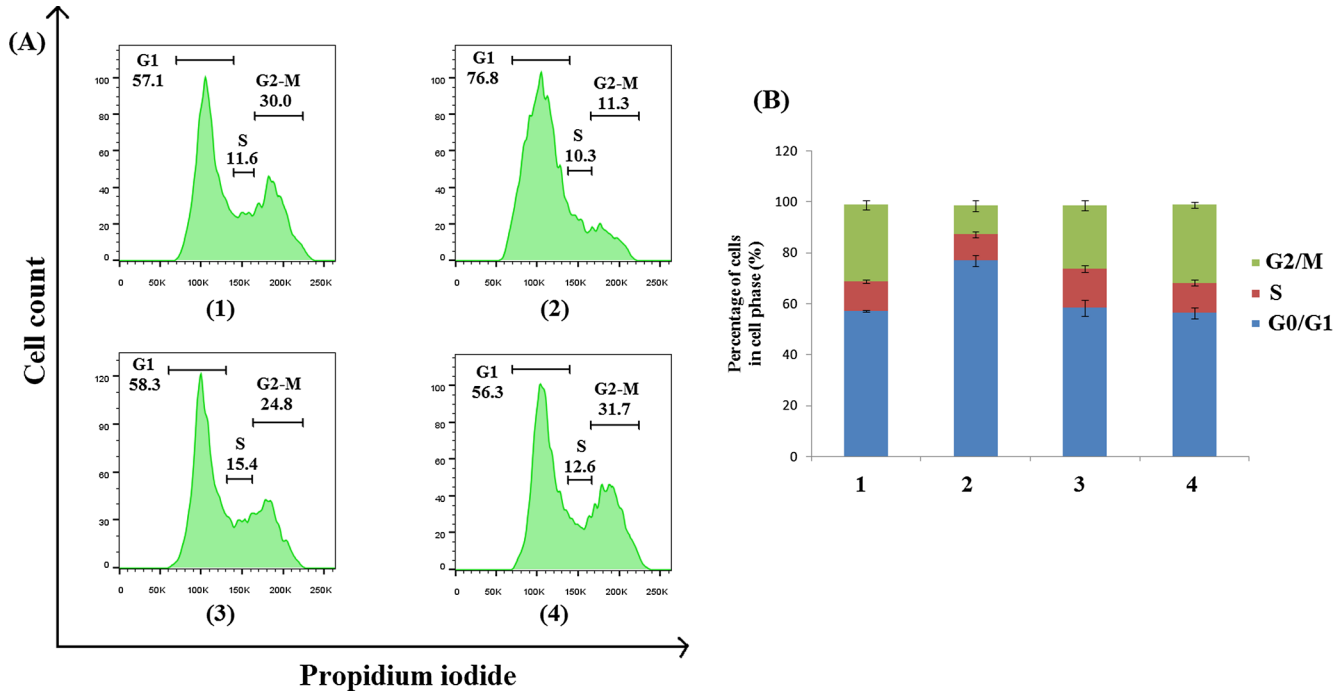

Fig. 8. Cell cycle arrest analysis of ligand-L treated C33A cervical cancer cells. (A) Flow cytometry analysis of treated C33A cervical cancer cells. (1) Control (2) ligand-L (5 μM) (3) ligand-L (5 μM) + Neocuproine (50 μM) (membrane permeable Cu(II) chelator) (4) ligand-L (5 μM) + NAC (1 mM) treatment. Representative figures of cell cycle distribution (G1, S, and G2-M) showing accumulation of ligand-L treated cells in G1 stage. (B) Bar graph representation showing percentage of cells in different cell phases after different treatments. Sets (1)-(4) correspond to the treatments mentioned above. Values are expressed as mean ± SEM of three independent experiments. All incubations were carried out for 24 h at 37 °C.

generation was abrogated both by neocuproine and NAC (Fig. 6A).

To evaluate superoxide anion ($O_2^{\cdot-}$) generation, cells were incubated with a fluorescent probe DHE which is specific to superoxide anion and reacts minimally to H_2O_2 [55]. Superoxide production was elevated 1.84-fold as compared to control in ligand-L treated cells (at IC_{50} concentration) (Fig. 6B) and was suppressed on addition of NAC and

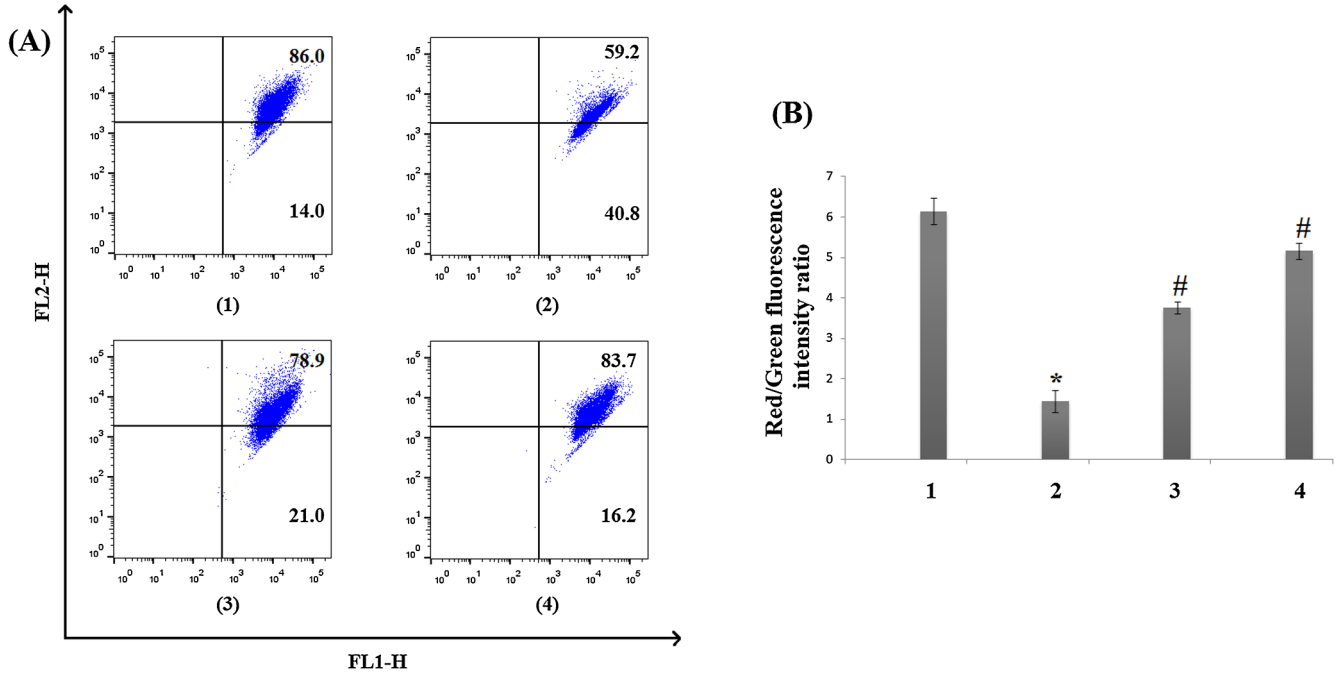

Fig. 9. Ligand-L induces changes in the mitochondrial membrane potential. (A) Flow cytometry analysis of treated C33A cervical cancer cells. (1) Control (2) ligand-L (5 μM) (3) ligand-L (5 μM) + Neocuproine (50 μM) (membrane permeable Cu(II) chelator) (4) ligand-L (5 μM) + NAC (1 mM) treatment. Representative dot plots showing the loss of mitochondrial membrane potential assessed from monomeric (green fluorescence indicated by FL1-H) and aggregate (red fluorescence indicated by FL2-H) forms of JC-1 fluorescence by flow cytometry. (B) Bar graph representation showing red/green fluorescence intensity ratio after different treatments. Sets (1)-(4) correspond to the treatments mentioned above. Values are expressed as mean ± SEM of three independent experiments. *P < 0.05 with respect to control group and #P < 0.05 with respect to 5 μM ligand-L treated cells. All incubations were carried out for 24 h at 37 °C.

neocuproine (Fig. 6B). Based on the above observations, the results suggest that ligand-L induces ROS generation through its ability to interact with cellular copper ions. Therefore, we predict that ligand-L is involved in redox cycling of Cu(II) that increases the intracellular ROS levels.

Fig. 6C demonstrates the results of hydroxyl radical production by ligand-L in the absence and presence of Cu(II) ions. Ligand-L alone (at IC_{50} concentration) did not produce any significant hydroxyl radicals (Fig. 6C). However, in the presence of Cu(II) significant hydroxyl radical production was observed and the hydroxyl radical generation was suppressed on addition of thiourea and neocuproine (Fig. 6C).

3.7. Apoptosis induction in C33A cells by ligand-L

Apoptosis in treated C33A cells was quantified by FACS analysis after staining with Annexin V-FITC and propidium iodide (PI). Dot plot results showed that most of the control (untreated) cells were negative for both Annexin V and PI (annexin V- PI-) (> 90%), thereby indicating no cell damage and also no disruption of cell membrane (Fig. 7). Exposure of C33A cells to ligand-L resulted in significant increase in percentage of early apoptotic cells from 3.13% in untreated group to 48.9% in ligand-L exposed cells. A similar pattern was observed in late apoptotic cells as well; the percentage of Annexin V + PI + cells was concomitantly increased from 0.76% in untreated cells to 5.97% in ligand-L treated cells. Incubation with membrane permeant copper chelator neocuproine strongly reduced the percentage of cells in early (reduced to 20.2%) and late (reduced to 1.96%) apoptosis. It was also observed that free radical scavengers NAC significantly reduced apoptosis in ligand-L treated cells.

3.8. Effect of ligand-L on cell cycle arrest

In order to determine whether ligand-L can affect cell cycle progression, propidium iodide based FACS analysis was performed to analyze the percentage of G0/G1, S and G2/M cell population in treated C33A cells (Fig. 8). C33A cells treated with IC_{50} concentration showed an increase in G0/G1 cell population (76.8%) compared with 57.1% in the control. This increase in the G0/G1 phase cell population was accompanied by concomitant decrease in G2/M phase of the cell cycle from control (30.0%) to treated C33A cells (11.3%). These results indicate that ligand-L induced cell cycle arrest at the G0/G1 phase. Further, in a different set of experiment, cell cycle arrest was suppressed significantly both by neocuproine and NAC. This suggests that interaction of ligand-L with copper and ROS generation play a central role in cell cycle arrest.

3.9. Ligand-L induces changes in the mitochondrial membrane potential ($\Delta\Psi_m$)

To explore the effect of ligand-L on mitochondrial membrane potential, C33A cells were incubated with IC_{50} concentration of ligand-L for 24 h and JC-1 assay was performed. Representative dot plots for FL2-H indicates red fluorescence (indicator of intact membrane potential) and FL1-H indicates green fluorescence (indicator of loss of

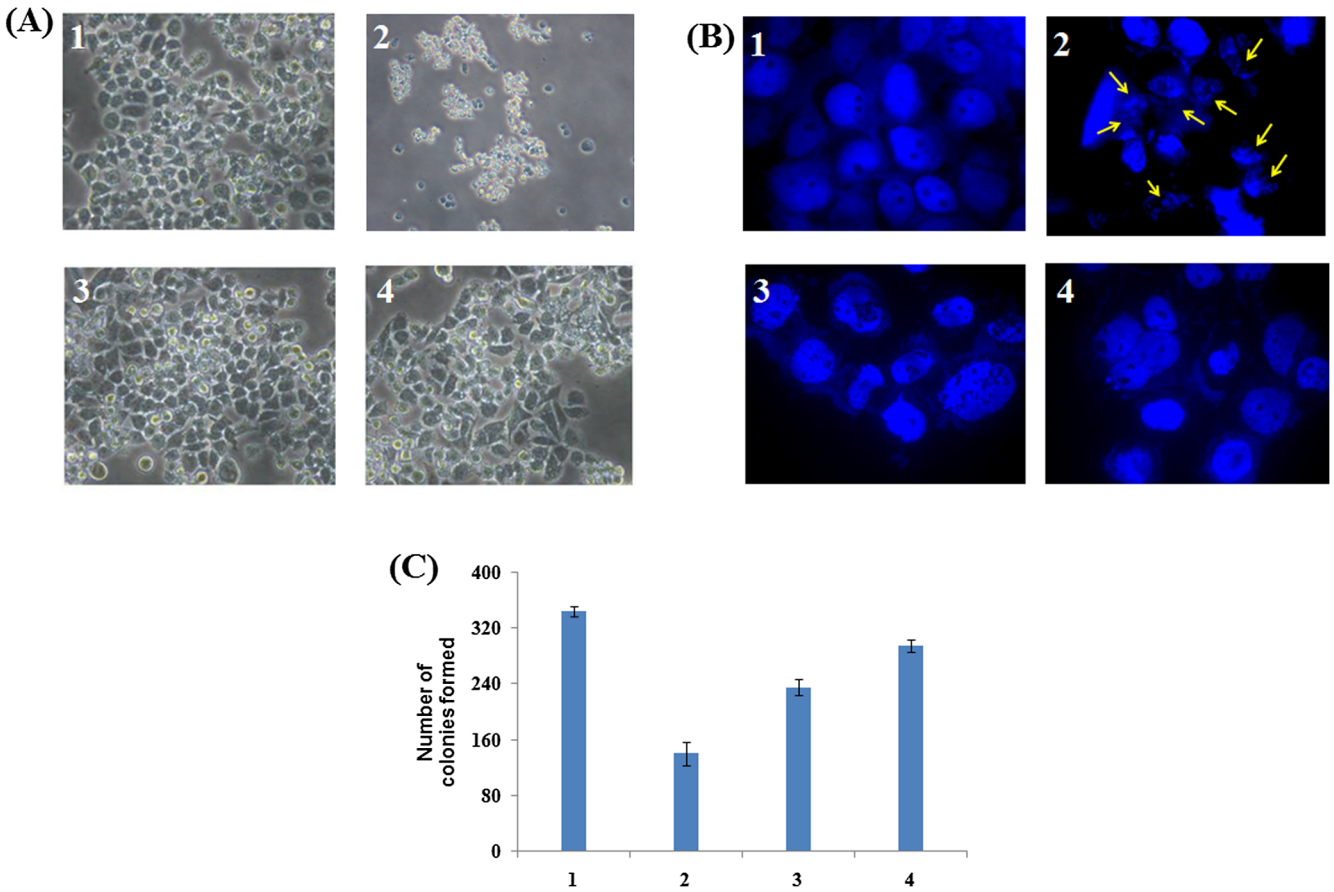

Fig. 10. (A) Morphological assessment of control and ligand-L treated C33A cervical cancer cells. Panel 1: Control cells. Panel 2: Ligand-L (5 μM). Panel 3: Ligand-L (5 μM) + Neocuproine (50 μM) (membrane permeable Cu(II) chelator). Panel 4: Ligand-L (5 μM) + NAC (1 mM) treatment. (B) DAPI staining for apoptosis analysis by ligand-L treatment. Panel 1: Control cells. Panel 2: Ligand-L (5 μM). Panel 3: Ligand-L (5 μM) + Neocuproine (50 μM) (membrane permeable Cu(II) chelator). Panel 4: Ligand-L (5 μM) + NAC (1 mM) treatment. Arrows in Panel 2 represent DNA fragmentation. (C) Clonogenic assay was performed to investigate the effect of ligand-L treatment on clone forming ability of C33A cells. (1): Control cells. (2): Ligand-L (5 μM). (3): Ligand-L (5 μM) + Neocuproine (50 μM) (membrane permeable Cu(II) chelator). (4): Ligand-L (5 μM) + NAC (1 mM) treatment. All incubations were carried out for 24 h at 37 °C.

mitochondria membrane potential) as shown in Fig. 9. Results showed that untreated cells exhibited largely red fluorescence indicating intact mitochondrial membrane potential (Fig. 9, Panel 1). However, on addition of ligand-L, there is an increase in number of cells showing green fluorescence (Fig. 9, Panel 2). This clearly shows that ligand-L disrupts mitochondrial membrane potential, indicating its potent apoptotic activity. Incubation of C33A cells with neocuproine largely decreases the disruption of mitochondrial membrane potential (Fig. 9, Panel 3). Similarly, the presence of free radical scavenger (NAC) also resulted in maintaining the membrane potential (Fig. 9, Panel 4). These results suggest that interaction of ligand-L with copper and ROS generation are involved in inducing changes in mitochondrial membrane potential.

3.10. Morphological assessment and nuclear changes of Ligand-L C33A treated cells

Ligand-L induces morphological changes in C33A cells as shown in Fig. 10A. Upon treatment with ligand-L at IC_{50} concentration for 24 h, C33A cells resulted in cell shrinkage, formation of apoptotic bodies and reduction in anchorage from surface (Fig. 10A, Panel 2). All these effects were suppressed by neocuproine and NAC (Fig. 10A, Panels 3 and 4).

To further investigate apoptosis induction via ligand-L, nuclear morphology of treated cells was examined using DAPI staining. Apoptotic cells are characterised by chromatin condensation and DNA fragmentation [56]. In untreated cells, the nucleus was round without condensation or fragmentation (Fig. 10B, Panel 1). Like in apoptotic cells, treatment with ligand-L resulted in maximum DNA fragmentation (Fig. 10B, Panel 2). Chelation of copper ions by neocuproine inhibits DNA fragmentation and largely reverses the nucleus morphology to untreated control cells (Fig. 10B, Panel 3). Free radical scavengers (NAC) significantly inhibited DNA fragmentation thereby implicating the role of ROS in ligand-L induced apoptosis in C33A cells (Fig. 10B, Panel 4).

3.11. Ligand-L reduces clonogenic potential of C33A cells

Incubation with ligand-L at IC_{50} concentration greatly reduces the colony-forming ability of C33A cells as compared to control group (Fig. 10C). On the other hand, incubation with neocuproine and NAC did not result in the reduction of colony-forming ability of C33A cells as shown in Fig. 10C. These results suggest redox cycling of copper by ligand-L to generate ROS involved in reducing the clonogenic potential of C33A cells.

3.12. Effect of ligand-L on p53, p21, caspases, pro-apoptotic and anti-apoptotic molecules

To follow up the molecular mechanism by which ligand-L induces apoptosis, we studied the levels of proteins involved in apoptosis. Results showed that exposure of C33A cells to ligand-L up-regulated the expression of Bax (pro-apoptotic protein), whereas expression of Bcl-2 (anti-apoptotic protein) was down-regulated (Fig. 11). Both these effects were completely reversed (down-regulation of Bax and up-regulation of Bcl-2) in the presence of neocuproine and NAC (Fig. 11). Western blot analysis revealed that p53 expression was elevated after ligand-L treatment and suppressed in the presence of neocuproine and NAC (Fig. 11). Our results also revealed that protein levels of p21 were increased on treatment with ligand-L, whereas neocuproine and NAC reduces the expression of p21 in ligand-L treated C33A cells (Fig. 11).

To study the effect of ligand-L on cell cycle checkpoints, western blot analysis was performed on CDK2 and cyclin-E (G1/S transition dependent proteins). Treatment with ligand-L at IC_{50} concentration drastically reduces the expression of CDK2 and cyclin-E in C33A cells (Fig. 11). Interestingly, CDK2 and cyclin-E expression was up-regulated again in the presence of neocuproine and NAC (Fig. 11).

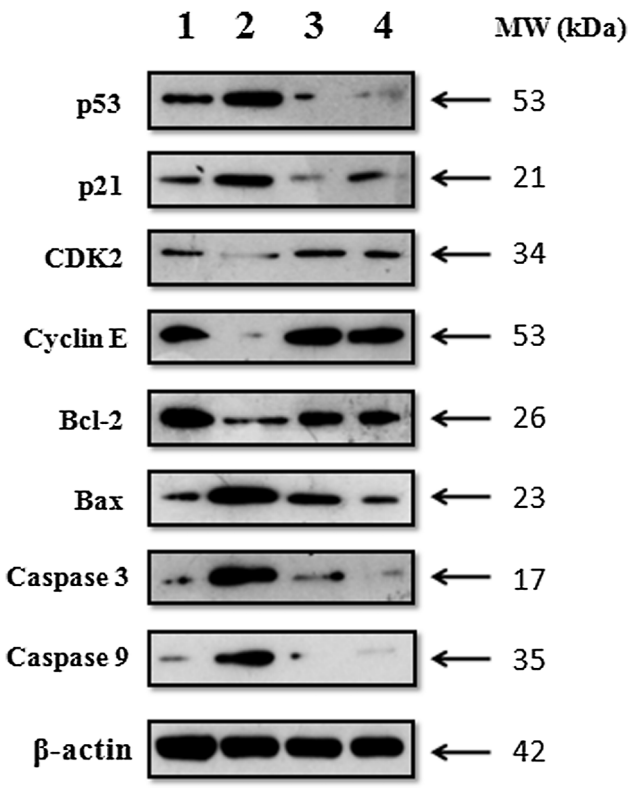

Fig. 11. Western blot showing the expression levels of cleaved caspases 3/9, Bax (pro-apoptotic), Bcl-2 (anti-apoptotic), cyclin E and CDK2 in C33A cervical cancer cells treated with ligand-L. (1) Control cells (2) ligand-L (5 μM) (3) ligand-L (5 μM) + Neocuproine (50 μM) (membrane permeable Cu(II) chelator) (4) ligand-L (5 μM) + NAC (1 mM) treatment. β-actin was used as a loading control.

Further, C33A cells induce the activation of caspases 3 and 9 after the treatment of ligand-L (Fig. 11). These results are consistent with mitochondrial membrane depolarisation (Fig. 9). As expected, the presence of neocuproine and NAC abolished the activation of caspases −3 and −9 in C33A cells (Fig. 11). Altogether, our results suggest that apoptosis-inducing effects of ligand-L in cervical cancer cells involve redox cycling of copper ions to generate ROS which leads to DNA fragmentation and apoptosis.

3.13. Molecular docking and MD simulation analyses

Details of molecular docking and clustering summary of each stage are summarized in Table 1. Docking studies confirmed that ligand-L preferably binds in the groove region of B-DNA and most part of ligand-L is present in the minor groove of B-DNA (Fig. 12A). However, tetrazole ring of ligand-L reaches to major groove region also and forms two hydrogen bonds with B-DNA. In total, ligand-L forms three hydrogen bonds with B-DNA (Fig. 12B) with binding energy −12.78 kcal/mol

Table 1
Molecular docking and clustering summary of ligand-L-DNA complex.

Parameters	Stage one docking	Stage two docking
Number of clusters formed	44	7
Population of maximum populated cluster[a]	19	75
Binding energy (kcal/mol)[b]	−12.02	−12.78
Inhibition constant[b]	1.55 nM	428.22 pM

[a] Out of 100 GA runs.
[b] Best pose from the maximum populated cluster.

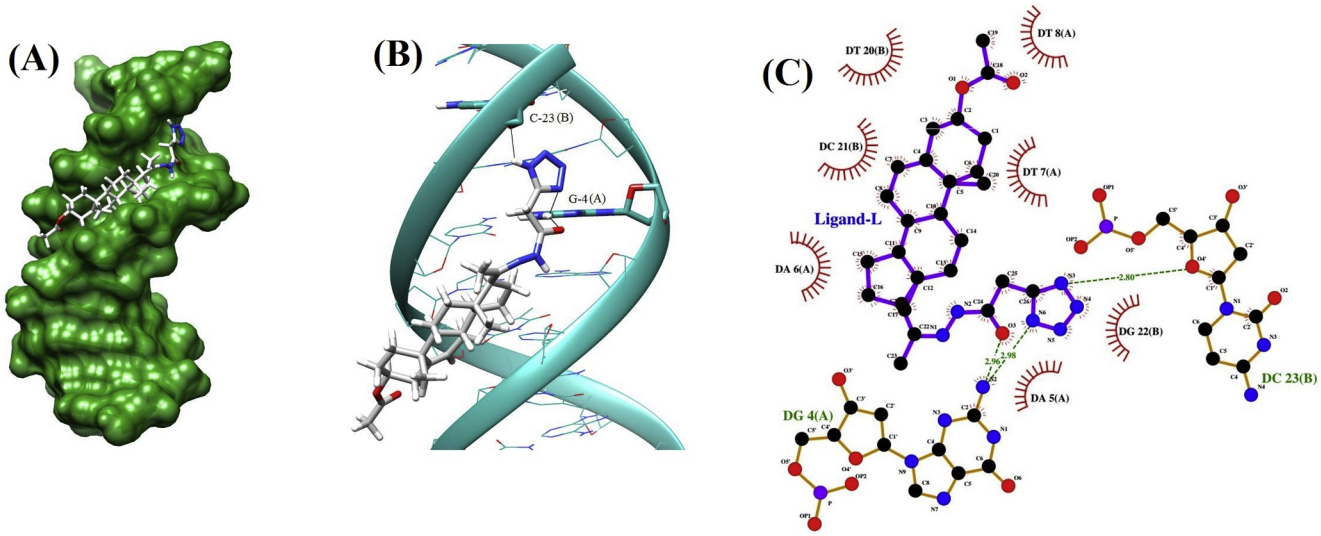

Fig. 12. (A) Preferred binding site of ligand-L on B-DNA analysed by molecular docking. Ligand-L binds in the groove region of the B-DNA. (B) Binding mode of ligand-L into B-DNA. Black lines represent hydrogen bonds. (C) Detailed interaction view of ligand-L with B-DNA generated by Ligplot.

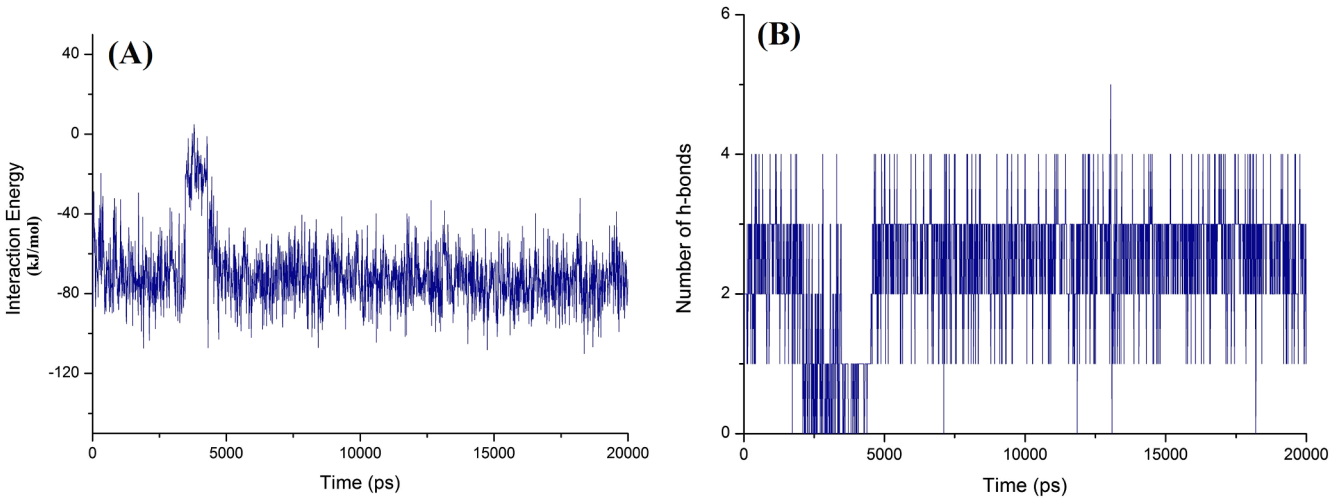

Fig. 13. Stability evaluation of docked ligand-L-DNA complex via MD simulations. (A) Interaction energy plot for 20 ns MD simulation of ligand-L with B-DNA. (B) Stability evaluation of ligand-L-DNA docked complex using hydrogen bonding pattern as a function of time.

and inhibition constant 428.22 pM. Ligplot revealed all the hydrophobic contacts and hydrogen bonds between the ligand-L and B-DNA (Fig. 12C). More negative interaction energy (> -10.0 kcal mol^{-1}) and lower inhibition constant (in pM) supports strong binding of ligand-L with B-DNA.

Further, MD simulation was performed to estimate the stability of the ligand-L-DNA docked complex. Interaction energy plot clearly illustrates overall stability of the complex till the end of MD run with an average energy -80 kJ/mol (Fig. 13A). The variation in interaction energy was found to be insignificant and was more stable from 4.5 ns to 20 ns. There was a slight fluctuation for 1 ns (from 3.5 ns to 4.5 ns), and this corresponds to the dissociation of ligand-L from the binding site of B-DNA. After 4.5 ns, the association between ligand-L and B-DNA was established again till the end of 20 ns long simulation. Corresponding changes were also noticed from the plot illustrating number of hydrogen bonds between Ligand-L and B-DNA (Fig. 13B). The hydrogen interaction number reaches five and for most of the time remains three or four in number. This illustration of greater hydrogen interaction numbers further confirms the greater stability of the ligand-L with B-DNA.

4. Discussion

Efficacy of chemotherapy is mainly limited due to side effects and drug resistance. Therefore, it is imperative to explore and synthesize effective anticancer compounds with lesser toxicity. Since steroid-based chemotherapeutic drugs possess higher bioavailability, non-toxic nature and less multi-drug resistance [18], therefore steroid-based derivatives with significant chemopreventive and therapeutic efficacy should be developed against malignancies. In this work, pregnenolone acetate-based tetrazole derivative (ligand-L) was synthesized against human cervical cancer C33A cells. Our study demonstrates that ligand-L inhibited cell viability of C33A cells in a dose-dependent manner. Ligand-L treated C33A cells exhibited cell shrinkage, formation of apoptotic bodies and reduction in anchorage from surface. Ligand-L induced apoptosis of C33A cells was demonstrated by Annexin V-FITC/PI staining, DNA fragmentation and caspase 9/3 activation.

Our study has also demonstrated that ligand-L treated C33A cells are associated with up-regulation of Bax and down-regulation of Bcl-2, leading to an increase in the ratio of Bax/Bcl-2. This increase in Bax/Bcl-2 ratio plays a crucial role in mitochondrial-mediated apoptosis [57]. Pro-apoptotic protein Bax translocates to the mitochondria and

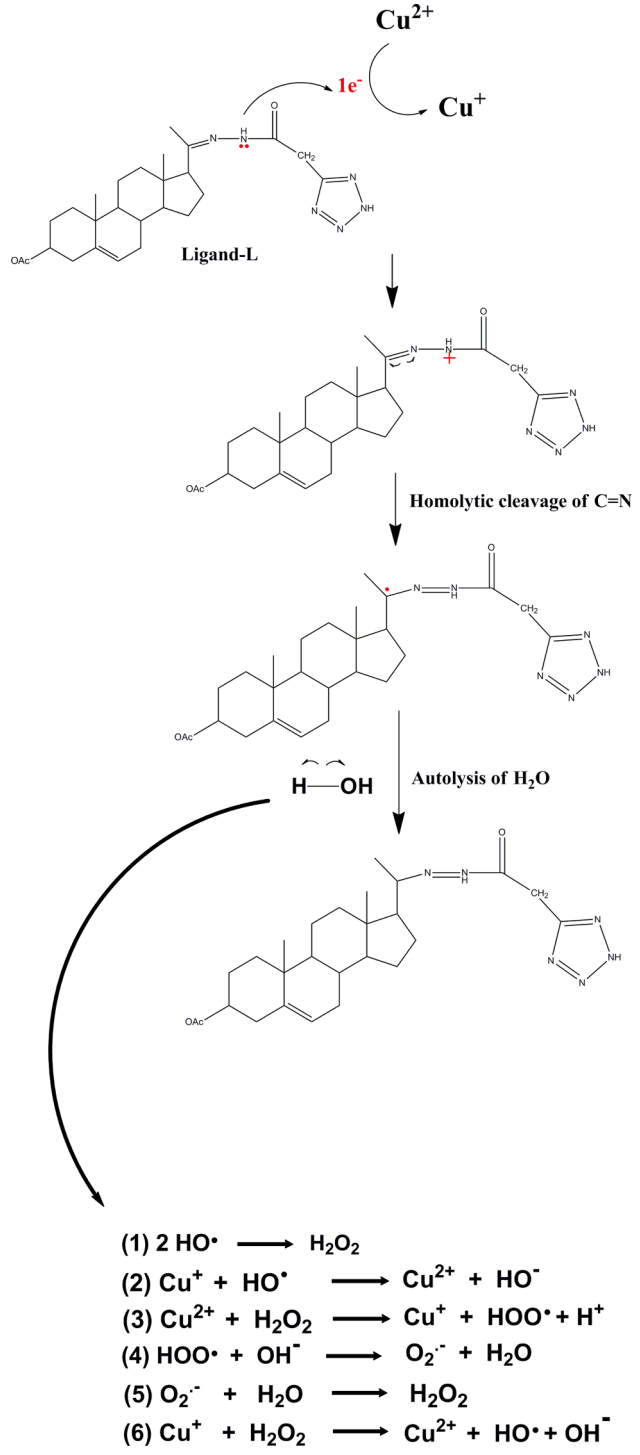

Fig. 14. Putative reaction mechanism of Cu(II)-ligand-L interaction. Production of hydroxyl radicals, superoxide anions and hydrogen peroxide via Cu(II)-ligand-L interaction leads to DNA damage and apoptosis.

integrates into the outer mitochondrial membrane, thereby promotes the disruption of mitochondrial membrane permeability ($\Delta\psi_m$) and ultimately caspase 3 activation [58]. As evident from the results, loss of $\Delta\psi_m$ was observed in C33A cells treated with ligand-L. Taken together, these results suggest that mitochondrial-mediated apoptotic pathway is involved in ligand-L induced C33A cell death.

Increased ROS production leads to DNA damage, thereby causing damaged cells to enter cell cycle arrest to facilitate DNA repair or induce apoptosis in excessively damaged cells [59]. Excessive DNA damage can activate p53 which either directs the cell to cell cycle arrest at G1/S via cyclin-dependent kinase (CDK) inhibitor p21 or promotes mitochondrial apoptosis by activating Bax protein [60,61]. Our results show that the expression of p53 was up-regulated in ligand-L treated cells. This is in agreement with the results of over-expression of Bax which is directly activated by p53 to initiate mitochondrial-mediated apoptosis. In addition, it was also found that there was an increase of p21 expression in ligand-L treated cells. Cell cycle analysis showed that ligand-L causes cell cycle arrest at G1/S phase via p21 inhibitor, indicating that cell cycle arrest by ligand-L is regulated by p53.

Compared to normal cells, cancer cells contain elevated copper levels, therefore, we hypothesize that hydrazone tetrazole-ring system of ligand-L would interact preferentially with Cu(II) ions and generate ROS via Fenton-like reactions [62,63]. As evident from results, addition of neocuproine and NAC (ROS scavenger) significantly suppressed ligand-L mediated DNA damage and consequent apoptosis in C33A cells. These results strongly suggest that chromatin-bound copper ions in all probability act as molecular target for ligand-L to propagate redox cycling leading to ROS generation. Thus, ROS generation via ligand-L and Cu(II) ions interaction leads to extensive DNA damage which in turn activate p53 protein necessary for mitochondrial-mediated apoptosis or cell cycle arrest in C33A cells.

Furthermore, we propose a putative reaction mechanism to explain the pro-oxidant effect of ligand-L on interaction with DNA-bound Cu(II) (Fig. 14). The –NH of hydrazone group of ligand-L donates an electron to Cu(II) to convert it into Cu(I). Later, homolytic cleavage of C=N followed by autolysis of water leads to the formation of hydroxyl radicals. Hydroxyl radicals thus formed may combine with each other to form hydrogen peroxide. Hydrogen peroxide may further react with Cu (II) to form superoxide anion (via hydroperoxyl radical) and Cu(II) is reduced back to Cu(I). Superoxide anion may also react with water to form more hydrogen peroxide. Cu(I) may further react with hydrogen peroxide to form more hydroxyl radicals and Cu(I) is again converted to Cu(II), thereby continuing the redox cycle. Since intracellular copper is chromatin-bound, ligand-L can interact with bound copper ions to form free radicals in close proximity of DNA that causes oxidative DNA damage. It has also not escaped our notice that hydroxyl radicals which are most electrophilic with high reactivity and hence most damaging to DNA are also generated in the Cu(II)-ligand-L reaction. This observation was established experimentally using $^{\cdot}$OH radical assay on ligand-L treatment in the presence of Cu(II) ions.

Generation of oxygen radicals in close proximity of DNA leads to strand scission [64–66]. Such a pro-oxidant activity of ligands is preceded by their association with DNA, followed by the formation of free radicals at that site [67]. Therefore, ligand-L in all probability should interact with chromatin-bound Cu(II) and DNA to form Cu(II)-DNA-ligand-L ternary complex to mediate the process of free radical generation. Further, it is important to note that among the oxygen radicals; the hydroxyl radical is the most electrophilic with high reactivity and therefore possesses a small diffusion radius. Therefore, ligand-L should interact strongly and have a prolonged residence time in the binding cavity of DNA to facilitate its strong association with DNA and Cu(II) ions to mediate ROS generation. Based on the results of MD simulation, we predict that ligand-L may act as a better lead molecule as it strongly interacts (3 or 4H-bonding) with the DNA molecule and hence will participate in redox cycling of Cu(II) ions to generate oxygen radicals in the proximity of DNA.

In summary, the present results show that ligand-L and Cu(II) interaction leads to selective cytotoxic action against cervical cancer cells and the cell death is due to redox cycling of copper and generation of intracellular ROS. Since cancer cells have significant accumulation of copper than normal cells, this endows ligand-L with an attractive antitumor activity with its selectivity towards malignancies. Thus, we propose copper dependent, ROS-mediated mechanism for the cytotoxic action of ligand-L in malignant cells. We expect that our study would be useful in establishing ligand-L as a lead molecule to synthesize new

anticancer drugs with better copper chelating and pro-oxidant properties.

Acknowledgements

The authors are grateful to Prof. M. Muneer (Department of Chemistry, AMU, Aligarh) who helped us in working out the reaction mechanism. We thank AIRF-JNU, New Delhi for NMR facility. The authors would like to thank the Chairperson, Dept. of Biochemistry, AMU, Aligarh for providing the necessary lab facilities. The financial support to AZ by DST-INSPIRE Junior Research Fellowship from the Govt. of India is acknowledged. This research did not receive any specific grant from funding agencies in the public, commercial, or not-for-profit sectors.

Appendix A. Supplementary material

Supplementary data to this article can be found online at https://doi.org/10.1016/j.bioorg.2019.03.031.

References

[1] M. Arbyn, X. Castellsagué, S. de Sanjosé, L. Bruni, M. Saraiya, F. Bray, J. Ferlay, Worldwide burden of cervical cancer in 2008, Ann. Oncol. 22 (2011) 2675–2686.
[2] H. Zur Hausen, Papillomavirus infections–a major cause of human cancers, Biochim. Biophys. Acta 1288 (1996) F55–F78.
[3] R. Vidya Priyadarsini, R. Senthil Murugan, S. Maitreyi, K. Ramalingam, D. Karunagaran, S. Nagini, The flavonoid quercetin induces cell cycle arrest and mitochondria-mediated apoptosis in human cervical cancer (HeLa) cells through p53 induction and NF-κB inhibition, Eur. J. Pharmacol. 649 (2010) 84–91.
[4] A.M. Florea, D. Büsselberg, Cisplatin as an anti-tumor drug: cellular mechanisms of activity, drug resistance and induced side effects, Cancers (Basel) 3 (2011) 1351–1371.
[5] J.J. Monsuez, J.C. Charniot, N. Vignat, J.Y. Artigou, Cardiac side-effects of cancer chemotherapy, Int. J. Cardiol. 144 (2010) 3–15.
[6] D. Yoshida, Y. Ikeda, S. Nakazawa, Quantitative analysis of copper, zinc and copper/zinc ratio in selected human brain tumors, J. Neurooncol. 16 (1993) 109–115.
[7] M. Ebadi, S. Swanson, The status of zinc, copper, and metallothionein in cancer patients, Prog. Clin. Biol. Res. 259 (1988) 161–175.
[8] A. Nasulewicz, A. Mazur, A. Opolski, Role of copper in tumour angiogenesis–clinical implications, J. Trace Elem. Med. Biol. 18 (2004) 1–8.
[9] T.F. Kagawa, B.H. Geierstanger, A.H. Wang, P.S. Ho, Covalent modification of guanine bases in double-stranded DNA. The 1.2-A Z-DNA structure of d(CGCGCG) in the presence of CuCl2, J. Biol. Chem. 266 (1991) 20175–20184.
[10] G.J. Brewer, Copper lowering therapy with tetrathiomolybdate as an antiangiogenic strategy in cancer, Curr. Cancer Drug Targets 5 (2005) 195–202.
[11] Q. Pan, C.G. Kleer, K.L. van Golen, J. Irani, K.M. Bottema, C. Bias, M. De Carvalho, E.A. Mesri, M. Robins, R.D. Dick, G.J. Brewer, S.D. Merajver, Copper deficiency induced by tetrathiomolybdate suppresses tumor growth and angiogenesis, Cancer Res. 62 (2002) 4854–4859.
[12] C. Trejo-Solís, D. Jimenez-Farfan, S. Rodriguez-Enriquez, F. Fernandez-Valverde, A. Cruz-Salgado, L. Ruiz-Azuara, J. Sotelo, Copper compound induces autophagy and apoptosis of glioma cells by reactive oxygen species and JNK activation, BMC Cancer 12 (2012) 156.
[13] A. Prisecaru, V. McKee, O. Howe, G. Rochford, M. McCann, J. Colleran, M. Pour, N. Barron, N. Gathergood, A. Kellett, Regulating bioactivity of Cu^{2+} bis-1,10-phenanthroline artificial metallonucleases with sterically functionalized pendant carboxylates, J. Med. Chem. 56 (2013) 8599–8615.
[14] R.K. Dubey, S. Oparil, B. Imthurn, E.K. Jackson, Sex hormones and hypertension, Cardiovasc. Res. 53 (2002) 688–708.
[15] K.A. Latham, A. Zamora, H. Drought, S. Subramanian, A. Matejuk, H. Offner, E.F. Rosloniec, Estradiol treatment redirects the isotype of the autoantibody response and prevents the development of autoimmune arthritis, J. Immunol. 171 (2003) (2003) 5820–5827.
[16] P.J. Sheridan, K. Blum, M. Trachtenberg, Steroid Receptors and Disease, Marcel Dekker, New York, 1988, pp. 289–564.
[17] V.K. Moudgil, Steroid Receptors in Health and Disease, Plenum Press, New York/London, 1987.
[18] A.H. Banday, B.P. Mir, I.H. Lone, K.A. Suri, H.M. Kumar, Studies on novel D-ring substituted steroidal pyrazolines as potential anticancer agents, Steroids 75 (2010) 805–809.
[19] M. Iqbal Choudhary, M. Shahab Alam, Yousuf S Atta-Ur-Rahman, Y.C. Wu, A.S. Lin, F. Shaheen, Pregnenolone derivatives as potential anticancer agents, Steroids 76 (2011) 1554–1559.
[20] A.H. Banday, S.A. Shameem, B.D. Gupta, H.M. Kumar, D-ring substituted 1,2,3-triazolyl 20-keto pregnenanes as potential anticancer agents: synthesis and biological evaluation, Steroids 75 (2010) 801–804.
[21] R.M. Mohareb, F. Al-Omran, Reaction of pregnenolone with cyanoacetylhydrazine: novel synthesis of hydrazide-hydrazone, pyrazole, pyridine, thiazole, thiophene derivatives and their cytotoxicity evaluations, Steroids 77 (2012) 1551–1559.
[22] R.M. Mohareb, W.W. Wardakhan, G.A. Elmegeed, R.M. Ashour, Heterocyclizations of pregnenolone: novel synthesis of thiosemicarbazone, thiophene, thiazole, thieno [2,3-b]pyridine derivatives and their cytotoxicity evaluations, Steroids 77 (2012) 1560–1569.
[23] B. Le Bourdonnec, E. Meulon, S. Yous, J.F. Goossens, R. Houssin, J.P. Hénichart, Synthesis and pharmacological evaluation of new pyrazolidine-3, 5-diones as AT(1) angiotensin II receptor antagonists, J. Med. Chem. 43 (2000) 2685–2697.
[24] L.W. Tremblay, H. Xu, J.S. Blanchard, Structures of the Michaelis complex (1.2 Å) and the covalent acyl intermediate (2.0 Å) of cefamandole bound in the active sites of the Mycobacterium tuberculosis β-lactamase K73A and E166A mutants, Biochemistry 49 (2010) 9685–9687.
[25] S.D. Diwakar, S.S. Bhagwat, M.S. Shingare, C.H. Gill, Substituted 3-((Z)-2-(4-nitrophenyl)-2-(1H-tetrazol-5-yl) vinyl)-4H-chromen-4-ones as novel anti-MRSA agents: synthesis, SAR, and in-vitro assessment, Bioorg. Med. Chem. Lett. 18 (2008) 4678–4681.
[26] A. Rajasekaran, P.P. Thampi, Synthesis and analgesic evaluation of some 5-[beta-(10-phenothiazinyl)ethyl]-1-(acyl)-1,2,3,4-tetrazoles, Eur. J. Med. Chem. 39 (2004) 273–279.
[27] C.N.S.S.P. Kumar, D.K. Parida, A. Santhoshi, A.K. Kota, B. Sridhar, V.J. Rao, Synthesis and biological evaluation of tetrazole containing compounds as possible anticancer agents, Med. Chem. Commun. 2 (2011) 86–492.
[28] T. Ichikawa, T. Kitazaki, Y. Matsushita, M. Yamada, R. Hayashi, M. Yamaguchi, Y. Kiyota, K. Okonogi, K. Itoh, Optically active antifungal azoles. XII. Synthesis and antifungal activity of the water-soluble prodrugs of 1-[(1R,2R)-2-(2,4-difluorophenyl)-2-hydroxy-1-methyl-3-(1H–1,2,4-triazol-1-yl)propyl]-3-[4-(1H-1-tetrazolyl)phenyl]-2-imidazolidinone, Chem. Pharm. Bull. (Tokyo) 49 (2001) 1102–1109.
[29] R.J. MacFadyen, M. Tree, A.F. Lever, J.L. Reid, Effects of the angiotensin II receptor antagonist Losartan (DuP 753/MK 954) on arterial blood pressure, heart rate, plasma concentrations of angiotensin II and renin and the pressor response to infused angiotensin II in the salt-deplete dog, Clin. Sci. (Lond.) 83 (1992) 549–556.
[30] M. Karaman, S. Balta, A.Y. Seyit Ahmet, M. Cakar, I. Naharci, S. Demirkol, T. Celik, Z. Arslan, O. Kurt, N. Kocak, H. Sarlak, S. Demirbas, F. Bulucu, E. Bozoglu, The comparative effects of valsartan and amlodipine on vWf levels and N/L ratio in patients with newly diagnosed hypertension, Clin. Exp. Hypertens. 35 (2013) 516–522.
[31] M. Bauer, R.K. Harris, R.C. Rao, D.C. Apperley, C.A. Rodger, NMR study of desmotropy in Irbesartan, a tetrazole-containing pharmaceutical compound, J. Chem. Soc. Perkin Trans. 2 (1998) 475–482.
[32] C.H. Lee, J.W. Liu, C.C. Li, C.C. Chien, Y.F. Tang, L.H. Su, Spread of ISCR1 elements containing blaDHA-$_1$ and multiple antimicrobial resistance genes leading to increase of flomoxef resistance in extended-spectrum-beta-lactamase-producing Klebsiella pneumonia, Antimicrob. Agents Chemother. 55 (2011) 4058–4063.
[33] L. Pochini, M. Galluccio, D. Scumaci, N. Giangregorio, A. Tonazzi, F. Palmieri, C. Indiveri, Interaction of beta-lactam antibiotics with the mitochondrial carnitine/acylcarnitine transporter, Chem. Biol. Interact. 173 (2008) 187–194.
[34] P.N. Gaponik, S.V. Voitekhovich, O.A. Ivashkevich, Metal derivatives of tetrazoles, Russ. Chem. Rev. 75 (2006) 507–539.
[35] IUPAC, Joint Commission on Biochemical Nomenclature (JCBN). Nomenclature of steroids, Pure Appl. Chem. 61 (1989) 1783–1822.
[36] IUPAC, Joint Commission on Biochemical Nomenclature (JCBN). The nomenclature of steroids, Recommendations 1989. Eur. J. Biochem. 186 (1989) 429–458.
[37] C.V. Kumar, E.H. Asuncion, DNA binding studies and site selective fluorescence sensitization of an anthryl probe, J. Am. Chem. Soc. 115 (1993) 8547–8553.
[38] Z. Li, X. Yang, S. Dong, X. Li, DNA breakage induced by piceatannol and copper(II): mechanism and anticancer properties, Oncol. Lett. 3 (2012) 1087–1094.
[39] V. Karthick, K. Ramanathan, V. Shanthi, R. Rajasekaran, Identification of potential inhibitors of H5N1 influenza A virus neuraminidase by ligand-based virtual screening approach, Cell Biochem. Biophys. 66 (2013) 657–669.
[40] C. Southan, A. Stracz, Extracting and connecting chemical structures from text sources using chemicalize.org, J. Cheminform. 5 (2013) 20.
[41] B.L. Pool-Zobel, C. Guigas, R. Klein, C. Neudecker, H.W. Renner, P. Schmezer, Assessment of genotoxic effects by lindane, Food Chem. Toxicol. 31 (1993) 271–283.
[42] T. Mosmann, Rapid colorimetric assay for cellular growth and survival: application to proliferation and cytotoxicity assays, J. Immunol. Methods 65 (1983) 55–63.
[43] H. Wang, J.A. Joseph, Quantifying cellular oxidative stress by dichlorofluorescein assay using microplate reader, Free Radic. Biol. Med. 27 (1999) 612–616.
[44] S. Dikalov, U. Landmesser, D.G. Harrison, Geldanamycin leads to superoxide formation by enzymatic and non-enzymatic redox cycling. Implications for studies of Hsp90 and endothelial cell nitric-oxide synthase, J. Biol. Chem. 277 (2002) 25480–25485.
[45] G.J. Quinlan, J.M. Gutteridge, Oxygen radical damage to DNA by rifamycin SV and copper ions, Biochem. Pharmacol. 36 (1987) 3629–3633.
[46] R. Kapoor, P. Kakkar, Protective role of morin, a flavonoid, against high glucose induced oxidative stress mediated apoptosis in primary rat hepatocytes, PLoS One 7 (2012) e41663.
[47] A.H. Wyllie, J.F. Kerr, A.R. Currie, Cell death: the significance of apoptosis, Int. Rev. Cytol. 68 (1980) 251–306.
[48] G.M. Morris, R. Huey, W. Lindstrom, M.F. Sanner, R.K. Belew, D.S. Goodsell, A.J. Olson, Autodock4 and AutoDockTools4: automated docking with selective receptor flexibility, J. Comput. Chem. 30 (2009) 2785–2791.
[49] M.F. Sanner, Python: a programming language for software integration and development, J. Mol. Graph. Model 17 (1999) 57–61.

[50] E.F. Pettersen, T.D. Goddard, C.C. Huang, G.S. Couch, D.M. Greenblatt, E.C. Meng, T.E. Ferrin, UCSF Chimera–a visualization system for exploratory research and analysis, J. Comput. Chem. 25 (2004) 1605–1612.
[51] R.A. Laskowski, M.B. Swindells, LigPlot+: multiple ligand-protein interaction diagrams for drug discovery, J. Chem. Inf. Model 51 (2011) 2778–2786.
[52] M.J. Abraham, T. Murtola, R. Schulz, S. Páll, J.C. Smith, B. Hess, E. Lindahl, GROMACS: High performance molecular simulations through multi-levelparallelism from laptops to super computers, SoftwareX 1–2 (2015) 19–25.
[53] A.D. MacKerell Jr., N. Banavali, N. Foloppe, Development and current status of the CHARMM force field for nucleic acids, Biopolymers 56 (2000-2001) 257–265.
[54] V. Zoete, M.A. Cuendet, A. Grosdidier, O. Michielin, SwissParam: a fast force field generation tool for small organic molecules, J. Comput. Chem. 32 (2011) 2359–2368.
[55] V.P. Bindokas, J. Jordán, C.C. Lee, R.J. Miller, Superoxide production in rat hippocampal neurons: selective imaging with hydroethidine, J. Neurosci. 16 (1996) 1324–1336.
[56] A. Saraste, K. Pulkki, Morphologic and biochemical hallmarks of apoptosis, Cardiovasc. Res. 45 (2000) 528–537.
[57] A. Gross, J.M. McDonnell, S.J. Korsmeyer, BCL-2 family members and the mitochondria in apoptosis, Genes Dev. 13 (1999) 1899–1911.
[58] D.R. Green, Apoptotic pathways: ten minutes to dead, Cell 121 (2005) 671–674.
[59] C.J. Norbury, B. Zhivotovsky, DNA damage-induced apoptosis, Oncogene 23 (2004) 2797–2808.
[60] K.H. Vousden, X. Lu, Live or let die: the cell's response to p53, Nat. Rev. Cancer 2 (2002) 594–604.
[61] J.I. Leu, P. Dumont, M. Hafey, M.E. Murphy, D.L. George, Mitochondrial p53 activates Bak and causes disruption of a Bak-Mcl1 complex, Nat. Cell Biol. 6 (2004) 443–450.
[62] S.M. Hadi, S.F. Asad, S. Singh, A. Ahmad, Putative mechanism for anticancer and apoptosis-inducing properties of plant-derived polyphenolic compounds, IUBMB Life 50 (2000) 167–171.
[63] S.M. Hadi, S.H. Bhat, A.S. Azmi, S. Hanif, U. Shamim, M.F. Ullah, Oxidative breakage of cellular DNA by plant polyphenols: a putative mechanism for anticancer properties, Semin. Cancer Biol. 17 (2007) 370–376.
[64] A. Rahman, Shahabuddin, S.M. Hadi, J.H. Parish, Complexes involving quercetin, DNA and Cu(II), Carcinogenesis 11 (1990) 2001–2003.
[65] R. Bhat, S.M. Hadi, DNA breakage by tannic acid and Cu(II): sequence specificity of the reaction and involvement of active oxygen species, Mutat. Res. 313 (1994) 39–48.
[66] H. Ahsan, S.M. Hadi, Strand scission in DNA induced by curcumin in the presence of Cu(II), Cancer Lett. 124 (1998) 23–30.
[67] W.A. Pryor, Why is the hydroxyl radical the only radical that commonly adds to DNA? Hypothesis: it has a rare combination of high electrophilicity, high thermochemical reactivity, and a mode of production that can occur near DNA, Free Radic. Biol. Med. 4 (1988) 219–223.